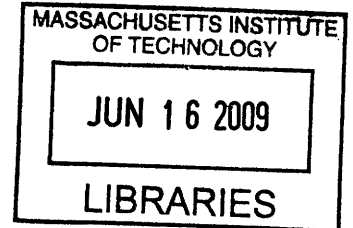# Vortex-Induced Motions of Marine Risers:

Straked Force Database Extraction

&

Transient Response Analysis

by

Filippos Chasparis

B.S.E. Operations Research & Financial Engineering

Princeton University

Submitted to the Department of Mechanical Engineering

in partial fulfillment of the requirements for the degree of

Master of Science in Naval Architecture and Marine Engineering

at the

Massachusetts Institute of Technology

June 2009

ARCHIVES

Author ....

Department of Mechanical Engineering

May 13, 2009

Certified by ....

Michael S. Triantafyllou

Professor of Mechanical and Ocean Engineering

Thesis Supervisor

Accepted by ....

David E. Hardt

Professor of Mechanical Engineering

Chairman, Department Committee on Graduate Students

To my Mother

Vortex-Induced Motions of Marine Risers:
Straked Force Database Extraction
&
Transient Response Analysis

Filippos Chasparis

Submitted to the Department of Mechanical Engineering
on June 2009 in partial fulfillment of the requirements for the degree of
Master of Science in Naval Architecture and Marine Engineering
at the Massachusetts Institute of Technology

Abstract

In part I of the thesis, we extend a methodology to extract a VIV hydrodynamic database from field data to accommodate partially straked cylinders. There are two databases, each consisting of the lift and added mass coefficients as functions of reduced velocity and amplitude of response; the first for the bare part of the riser, and the second for the straked part. First, the program VIVA together with nominal force databases obtained from laboratory hydrodynamic experiments is used in order to get an initial prediction of the riser response under a particular flow profile. The nominal databases are then altered in a systematic way until the new VIVA predicted response best matches the measured field response, thus resulting in optimal databases.

In part II of the thesis, we show using experimental data on a model riser that lock-in of long flexible risers placed in sheared or uniform cross-flows is a much richer phenomenon than lock-in of flexibly-mounted rigid cylinders under similar conditions. In particular, we find that the frequency content of the riser response may be either narrow-banded around a single dominant frequency (Type I response) or distributed along a relatively broad range of frequencies (Type II response). Distinct transition from Type I to Type II response, and vice versa, can occur several times within a single experimental record. Type I responses reveal features of a quasi-periodic oscillation, often accompanied by large 3rd harmonic components in the acceleration and strain signals, increased correlation length, stable riser trajectories, and monochromatic traveling or standing waves. Type II responses, on the other hand, are characterized by features of chaotic oscillation with small or non-existent 3rd harmonic components in the acceleration and strain signals, reduced correlation length, and a continuous spectrum.

Thesis Supervisor: Michael S. Triantafyllou
Title: Professor of Mechanical and Ocean Engineering, MIT

Acknowledgements

Contents

List of Figures

List of Tables

Motivation & Thesis Structure

The problem of vortex-induced vibrations

When a bluff body is placed in a fluid stream, large scale separation occurs, usually starting at the largest cross-flow dimension of the body. This can lead to a flow instability, which can eventually result in organized unsteady wake motion. Vortex shedding and wake turbulence induce fluctuating pressure gradients on the surface of the body causing it to oscillate. If the body is free to move, as the frequency of vortex shedding approaches one of its natural frequencies, lock-in occurs giving rise to oscillations which are termed vortex-induced vibrations (VIV). These vibrations are self-limiting in amplitude to about one body diameter, but can be of relatively high frequency, often resulting in significant fatigue damage.

Nowadays, the problem of vortex-induced vibrations is becoming increasingly important in view of the ongoing search for petroleum in deeper waters. In such water depths, long cylindrical structures are employed in order to extract oil from the seabed. These so-called marine risers are very expensive in design, construction, installation and maintenance. It is important, therefore, especially for deep and ultra-deep water applications, that riser fatigue damage be accurately estimated before installation.
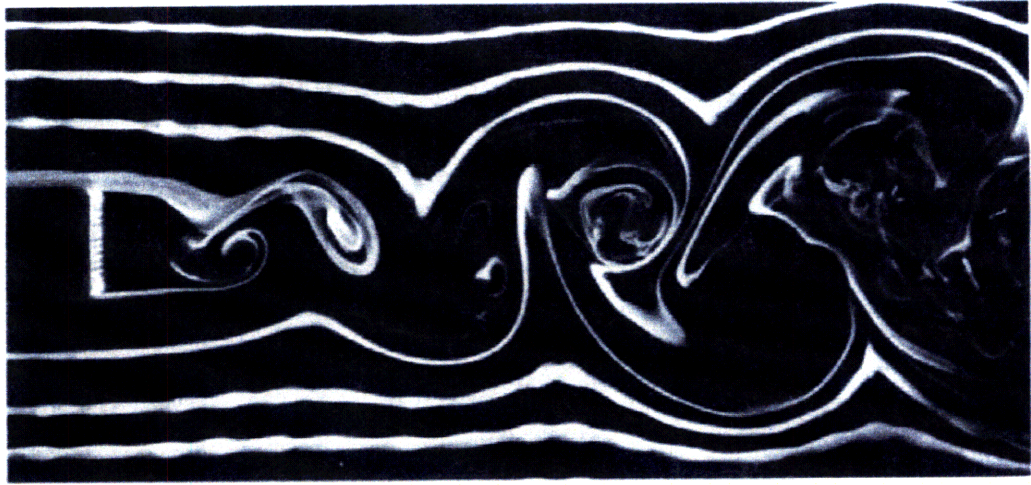
Figure 1: Formation of vortices behind a bluff body. (Figure from Bearman (1984).)
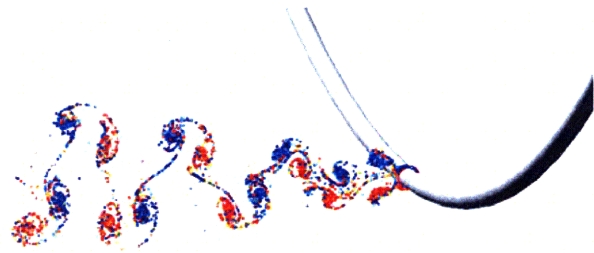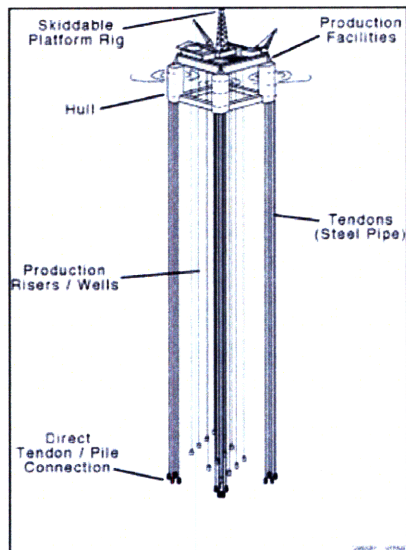
Figure 2: Long steel pipes are used by oil companies in order to extract petroleum from the ocean seabed; these pipes are often subject to strong currents and hence vortex-induced vibrations.

Thesis structure

This thesis is comprised of two separate parts: the first is on the extraction of optimal force databases from field data of straked risers; the second is on transient (as opposed to steady-state) behavior of risers.

Optimal straked database extraction

VIV-canceling devices (such as strakes) are often necessary to install when riser fatigue damage is estimated to be high. Strakes translate into higher installation costs, time delays, as well as increased drag (since they increase the effective riser diameter); hence, they are a necessary evil: strake coverage should be adequate to keep the fatigue life above an acceptable threshold, but at the same time use of strakes should be kept at a minimum.

The afore-mentioned reasons constitute VIV prediction of partially straked cylinders a very important issue in practice. Experiment-based predictive codes, such as the program VIVA (Triantafyllou (1998) and Triantafyllou, et al. (1999)), utilize strip theory and hydrodynamic databases obtained in laboratory tests using finite-span rigid cylinders in order to predict riser response. More specifically, VIVA assumes that riser response can be obtained via a strip theory approach, whereby the riser is subdivided into a large number of small-length, two-dimensional sections, whose hydrodynamic characteristics can be obtained from databases providing the lift coefficient in phase with velocity and the added mass coefficient as functions of non-dimensional velocity (or frequency) and non-dimensional amplitude. The questions that arise are the following. Can strip theory adequately model three-dimensional riser response? Is it possible to capture all fluid dynamic information in force databases? If yes, how can these databases be modified to account for changing Reynolds numbers and for other often unmodeled effects, such as the impacts of in-line motion?

In the first part of the thesis, we test the hypothesis that riser response can be adequately predicted under the above-mentioned assumptions. We apply a methodology for data extraction in order to obtain so-called universal straked databases, which allow us to accurately predict riser response for entire sets of data. The results reinforce the applicability of the strip theory approach,

and establish confidence in the hypothesis that appropriately modified force databases can take real riser effects into account.

Transient response analysis

As mentioned above, current semi-empirical prediction methods of vortex-induced vibrations of risers make heavy use of observations and results from vibrating rigid cylinders in the laboratory. Because of its importance to both theory and applications, testing of flexibly-mounted, relatively short-span rigid cylinders in cross-flow has become the canonical problem of flow-structure interaction. Lock-in is a central concept in rigid cylinder VIV: the wake frequency is first entrained or captured to coincide with the frequency of cylinder oscillation, and then the response locks-in with the natural frequency of the cylinder, which is modified by the rapidly changing effective added mass. As a result, nearly steady-state vibrations ensue.

On the other hand, experimental observations of real-sized risers show a very different picture. In particular, field data show that riser response may change significantly over time, even when external conditions, most importantly the flow profile, remain unchanged. In the second part of the thesis, we use experimental data to investigate the presence and importance of transition regions in riser VIV response. We show that there are two distinct types of response: the first is narrow-banded with significant higher harmonic components, and the second is distributed along a wider frequency range with several distinct peaks. We discuss defining characteristics of each type of response.

Part I

Optimal Straked Database Extraction

I.1   Introduction

This part is concerned with the problem of optimal force database extraction for partially straked marine risers. Following Irvine & Caughey (1974), Bliek (1984), Triantafyllou (1984), and Triantafyllou (1998), we model the riser as a taut inclined cable on which a fluid force is exerted. We proceed to decompose this hydrodynamic force into two parts: one in phase with velocity and one in phase with acceleration. This decomposition introduces a lift coefficient in phase with velocity and an added mass coefficient (lift coefficient in phase with acceleration), both of which depend on the frequency and amplitude of oscillation in a way that is far from trivial. Current practice is to rely on experiments to obtain detailed databases that tabulate the frequency and amplitude dependence of these force coefficients. Most extensive such databases for the case of bare cylinders were obtained by Gopalkrishnan (1993). Similar (but much sparser) databases for straked cylinders were presented by Dahl (2008). Mukundan (2008) developed a procedure that allowed him to derive optimal force databases for bare risers by successively altering the nominal databases of Gopalkrishnan until the theoretically predicted results best matched field data. We present a similar method for the case of partially straked risers.
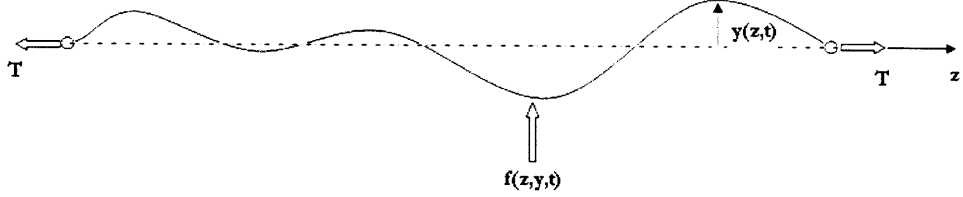
Figure I.1: Riser structural model.

I.2 The structural model

Consider a long cylindrical structure (a riser) of length L, diameter D, mass per unit length m, structural damping b and bending stiffness EI under tension T. In general, all of the structural properties may vary along the riser's span, but we shall assume them to be constant for simplicity. Let the structure be immersed in a fluid of density ρ and viscosity μ that moves with velocity $U(z)$ and exerts a force $f(z, y, t)$.[1] Then, allowing oscillations in one plane only, the linearized two-dimensional equation of motion is given by

$$m\frac{\partial^2 y(z,t)}{\partial t^2} + b\frac{\partial y(z,t)}{\partial t} - \frac{\partial}{\partial z}\left(T\frac{\partial y(z,t)}{\partial z}\right) + \frac{\partial^2}{\partial z^2}\left(EI\frac{\partial^2 y(z,t)}{\partial z^2}\right) = f(z,y,t).$$
(I.1)

We assume a solution of the form

$$y(z,t) = \Re\left(Y(z)e^{i\omega t}\right),$$
(I.2)

where $Y(z)$ is complex and ω is the frequency of (monochromatic) oscillation. Substituting (I.2) into (I.1) (and dropping the $\Re()$ for convenience) we obtain

$$\left[\left(-m\omega^2 + ib\omega\right)Y(z) - \frac{d}{dz}\left(T\frac{dY(z)}{dz}\right) + \frac{d^2}{dz^2}\left(EI\frac{d^2Y(z)}{dz^2}\right)\right]e^{i\omega t} = f(z,y,t).$$
(I.3)

---

[1]Note that the flow velocity and hydrodynamic force may vary along the riser's span; furthermore, the force exerted on the riser is a function of its motion.

I.3 The fluid force

We assume that the fluid force leads the displacement by a phase angle $\psi(z)$ and write

$$f(z, y, t) = \Re\left(F(z, y)e^{i(\omega t + \psi(z))}\right). \tag{I.4}$$

In view of (I.2), (I.4) may be written as

$$f(z, \omega, Y) = \Re\left(F(z, \omega, Y)e^{i\omega t}\left(\cos\psi(z) + i\sin\psi(z)\right)\right). \tag{I.5}$$

We substitute (I.5) into (I.3) (again dropping the $\Re()$ for convenience) to obtain

$$\left[\left(-m\omega^2 + ib\omega\right)Y(z) - \frac{d}{dz}\left(T\frac{dY(z)}{dz}\right) + \frac{d^2}{dz^2}\left(EI\frac{d^2Y(z)}{dz^2}\right)\right]e^{i\omega t}$$
$$= F(z, \omega, Y)\left(\cos\psi(z) + i\sin\psi(z)\right)e^{i\omega t}. \tag{I.6}$$

I.4 Dimensionless groups

At this point we have one equation (I.6) but three unknowns: ω, $Y(z)$ and $F(z, \omega, Y)$. For this reason, we introduce the so-called non-dimensional force coefficients, which allow us to relate the unknown quantities. More specifically, define

$$C_{lv}(z, \omega, Y) = \frac{F(z, \omega, Y)\sin\psi(z)}{[(1/2)\rho DU^2(z)]\frac{Y(z)}{|Y(z)|}} \tag{I.7}$$

to be the lift coefficient in phase with velocity, and

$$C_m(z, \omega, Y) = \frac{F(z, \omega, Y)\cos\psi(z)}{[(\pi/4)\rho D^2][\omega^2 Y(z)]} \tag{I.8}$$

to be the added mass coefficient (or lift coefficient in phase with acceleration). Substituting (I.7) and (I.8) into (I.6) and simplifying,

$$\frac{d^2}{dz^2}\left(EI\frac{d^2Y(z)}{dz^2}\right) - \frac{d}{dz}\left(T\frac{dY(z)}{dz}\right)$$
$$+ \left[\left(-m + (\pi/4)\rho D^2 C_m(z, \omega, Y)\right)\omega^2 + ib\omega\right]Y(z)$$
$$= i\left[(1/2)\rho DU^2(z)\right]\frac{Y(z)}{|Y(z)|}C_{lv}(z, \omega, Y). \tag{I.9}$$

23

Equation (I.9) and the appropriate boundary conditions define a non-linear boundary value problem, which, given $C_{lv}(z, \omega, Y)$ and $C_m(z, \omega, Y)$, can be solved (numerically, e.g. using VIVA.[2]) to obtain a countable set of frequencies ω_n and corresponding modes Y_n (where n is the mode number). It is not clear how one combines the different modes to obtain one final solution for the response of the riser. For our purposes, we assume that the dominant mode (i.e. the mode n for which $\max_z Y_n(z)$ attains its maximum) is sufficiently close to the real response and we do not distinguish between the two; in view of this, we denote their common frequency and mode by ω and Y respectively.

Let us, however, explore the solution a little further on dimensional grounds. By the Buckingham π theorem there should be 10 dimensionless groups, most of which can be obtained directly by inspection. More specifically, we may write

$$g\left(Y^*, z^*, L/D, Vr, m^*, \zeta, e, Re, C_{lv}, C_m\right) = 0, \qquad (I.10)$$

where

1. $Y^* = |Y|/D$ is the non-dimensional amplitude of oscillation,

2. $z^* = z/L$ is the non-dimensional span,

3. L/D is the aspect ratio,

4. $Vr = \frac{U}{(\omega/2\pi)D}$ is the reduced velocity,

5. $m^* = \frac{m}{(\pi/4)\rho D^2}$ is the mass ratio, i.e. the ratio of the mass of the structure to the mass of the displaced fluid,

6. $\zeta = \frac{b}{2(m^*+C_m)((\pi/4)\rho D^2)(\omega/2\pi)}$ is the structural damping ratio, i.e. the ratio of dissipative to hydrodynamic forces on the cable,

7. $e = \frac{EI}{TL^2}$ is the ratio of bending to tensile forces on the cable,

8. $Re = \frac{\rho U D}{\mu}$ is the Reynolds number, i.e. the ratio of fluid inertial to fluid viscous forces,

9. C_{lv} is the lift coefficient in phase with velocity defined in (I.7), and

10. C_m is the added mass coefficient defined in (I.8).

---

[2]For more on VIVA see Triantafyllou (2006).

For more on the physical significance of the above-mentioned non-dimensional quantities refer to Vandiver (1993) and Pantazopoulos (1994). In the sequel, we shall assume that all dimensionless groups in (I.10) are given or known except for Y^* and Vr (that we wish to solve for) and C_{lv} and C_m that we know only approximately. We shall then simplify the notation and write

$$g\left(Y^*, Vr, C_{lv}, C_m\right) = 0. \tag{I.11}$$

I.5 Nominal force databases for bare and straked risers

At this point, it should be evident that the C_{lv} and C_m coefficients play a vital role in the prediction of the motion of marine risers subject to VIV. For this reason, researchers have conducted detailed experiments in order to tabulate the dependence of these force coefficients on non-dimensional amplitude (Y^*) and reduced velocity (Vr) or (equivalently) reduced frequency ($1/Vr$).

The surface and contour plots shown in Figures I.2 and I.3 respectively were obtained by Gopalkrishnan (1993) and show $C_{lv}\left(Vr, Y^*\right)$ and $C_m\left(Vr, Y^*\right)$ for the case of a bare rigid cylinder undergoing forced vibrations at $Re \approx 10^4$. The most evident feature of these figures is the peak around the Strouhal frequency ($1/Vr = 1/6$). For a more detailed discussion see Gopalkrishnan (1993) and Mukundan (2008).

Similar databases for the case of straked cylinders (triple-start, pitch-to-diameter ratio equal to 15 and height-to-diameter ratio equal to 5) were obtained by Dahl (2008) at the MIT towing tank. These databases, which are much sparser than the bare ones, are shown in Figures I.4 - I.7. The basic feature to note here is that C_{lv} as a function of Y^* is downward sloping. Hence, the strakes act as pure sources of damping.

Henceforth, we shall refer to the bare and straked force databases presented in this section as the 'nominal' force databases.
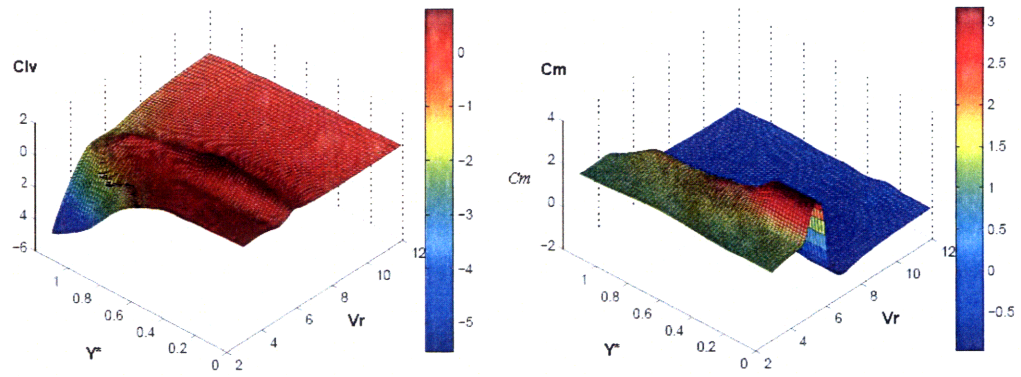
Figure I.2: $C_{lv}(Vr, Y^*)$ (left) and $C_m(Vr, Y^*)$ (right) surface plots for a bare rigid cylinder at $Re \approx 10^4$. (Figure adapted from Gopalkrishnan (1993).)
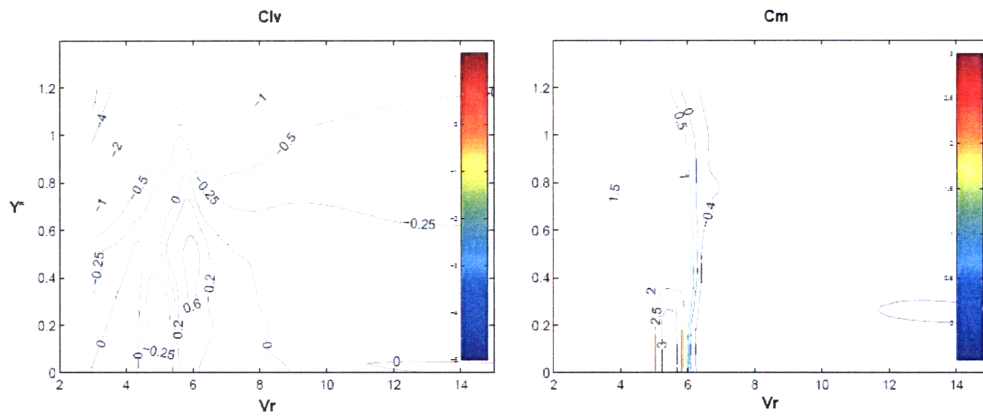
Figure I.3: $C_{lv}(Vr, Y^*)$ (left) and $C_m(Vr, Y^*)$ (right) contour plots for a bare rigid cylinder at $Re \approx 10^4$. (Figure adapted from Gopalkrishnan (1993).)
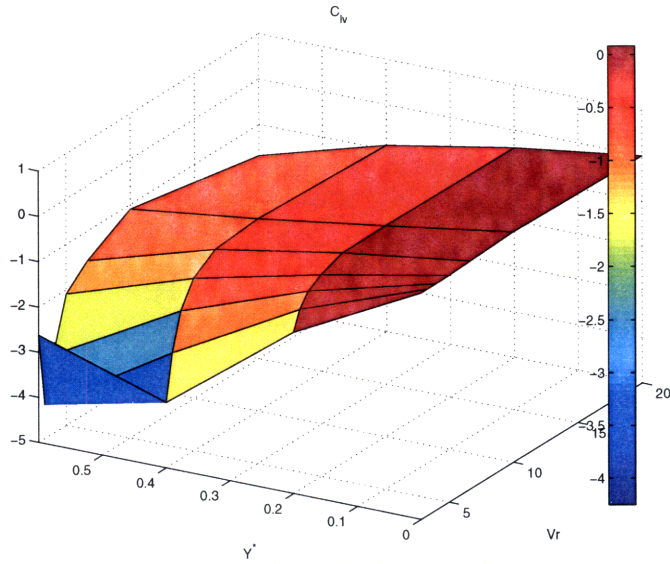
Figure I.4: $C_{lv}(Vr, Y^*)$ surface plot for a straked cylinder (triple-start, pitch-to-diameter ratio of 15 and height-to-diameter ratio of 5) at $Re \approx 10^4$. (Data for figure taken from Dahl (2008).)
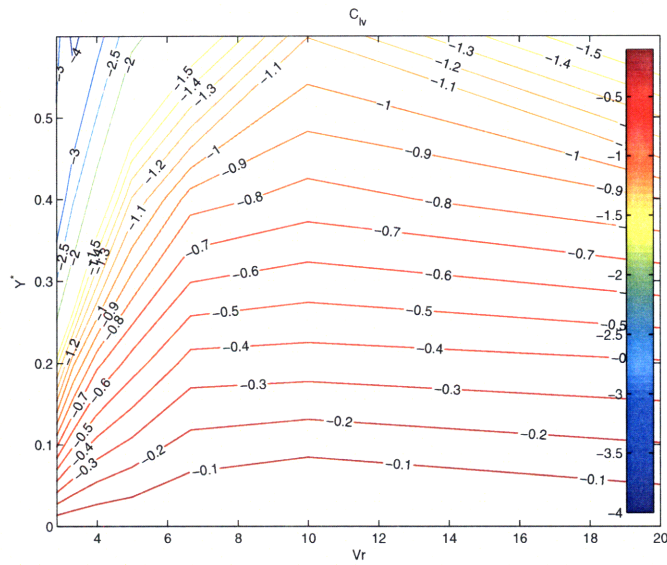
Figure I.5: $C_{lv}(Vr, Y^*)$ contour plot for a straked cylinder (triple-start, pitch-to-diameter ratio of 15 and height-to-diameter ratio of 5) at $Re \approx 10^4$. (Data for figure taken from Dahl (2008).)
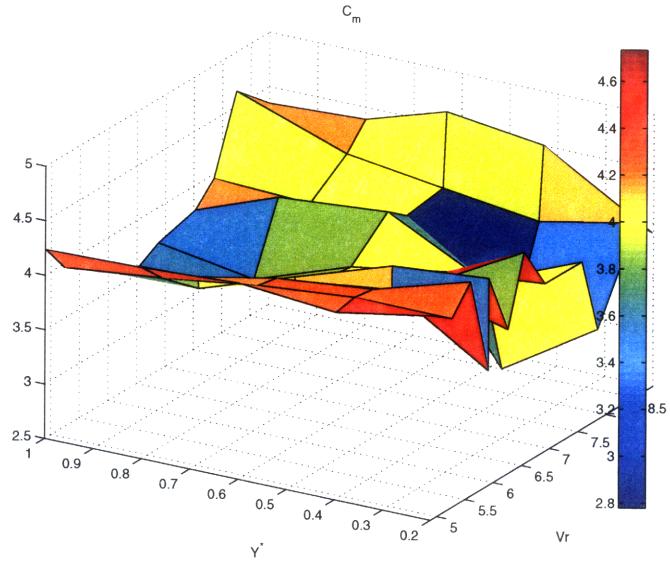
Figure I.6: $C_m\left(Vr, Y^*\right)$ surface plot for a straked cylinder (triple-start, pitch-to-diameter ratio of 15 and height-to-diameter ratio of 5) at $Re \approx 10^4$. (Data for figure taken from Dahl (2008).)
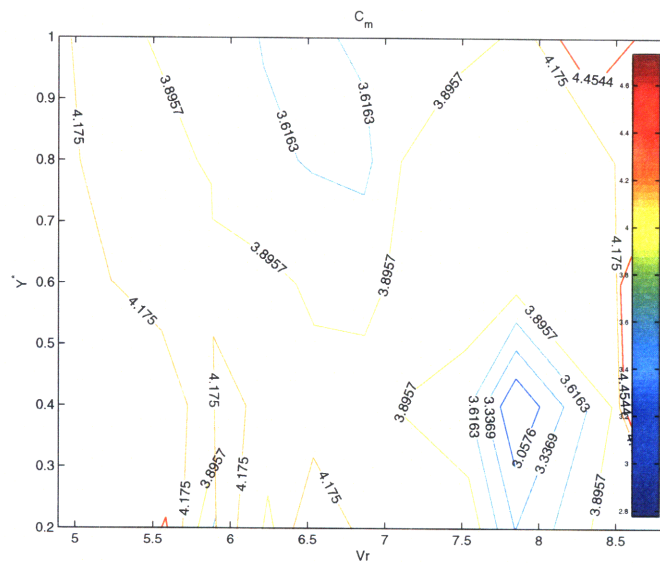
Figure I.7: $C_m\left(Vr, Y^*\right)$ contour plot for a straked cylinder (triple-start, pitch-to-diameter ratio of 15 and height-to-diameter ratio of 5) at $Re \approx 10^4$. (Data for figure taken from Dahl (2008).)

I.6 Experimental data

The nominal databases presented in the previous section were obtained by researchers by conducting experiments in towing tanks using model cylinders. This presents us with a few difficulties. First, the length of a model cylinder is typically much smaller than the length of a real riser (hence a Reynolds number discrepancy). Second, a model cylinder is (usually) rigid when a real riser is flexible. Third, the force databases are for cylinders oscillating in one plane only (the cross-flow) whereas real risers oscillate in two planes (cross-flow and in-line). It is known that Reynolds number and roughness effects have moderately large impact in the subcritical regime (Govardan & Williamson (2006)) and a large effect above the critical Reynolds number (Ding, et al. (2004)), while in-line response has a profound effect, influencing the amplitude of response and the force harmonic component content (Dahl, et al. (2007)).

Smogeli, et al. (2003) showed that force databases for marine risers can be obtained by scaling and translating the corresponding databases for model cylinders. This finding is the main idea on which our method for obtaining optimal force databases is based. We (numerically) solve (I.9) with the appropriate boundary conditions for a real riser using the nominal databases. We compare the theoretical results thus obtained with field observations for that same riser. We then modify the nominal databases in a systematic way (warping transformations) until theoretical and experimental results match.

For the purpose of obtaining optimal straked databases, we use data from the NDP VIV experiments. Appendix A contains a thorough description of the experimental setup; for the purpose of reading the current chapter, all one needs to know is that the experiment uses a $38m$-long, $27mm$-wide, tension-dominated model riser that is subject to uniform or linearly sheared velocity profiles. For the optimization, we use 19 datacases from the uniform straked 17_5_41 dataset, which spans a range of flow velocities from $0.5m/s$ to $2.3m/s$ (roughly in increments of $0.1m/s$). The available data for each datacase comprises of eight acceleration measurements along the length of the riser; these can be used to obtain the measured displacement rms values at the sensor locations.

I.7 The optimization model

We assume that optimal bare databases for the bare NDP experiments have already been obtained, either following Mukundan (2008) or a heuristic procedure outlined in Appendix B. The objective then is to obtain similar optimal straked databases for the partially straked NDP experiments.

I.7.1 Datacases

Let $\mathcal{D}$ be the set of all datacases, which we shall refer to as the dataset. A typical element (a datacase) of the set (the dataset) is $d \in \mathcal{D}$.

I.7.2 Databases and database transformations

Let $C_{lv,b}^{opt}$ and $C_{m,b}^{opt}$ be the available optimal bare databases. Similarly, let $C_{lv,s}^{nom}$ and $C_{m,s}^{nom}$ be the available nominal straked databases. Modified straked databases are obtained by appropriately scaling and translating the nominal straked databases. We shall denote such modified databases by $C_{lv,s}^{mod}$, $C_{m,s}^{mod}$ and the warping transformation that produces them by $\phi(\cdot)$. We then write

$$\phi : \left(C_{lv,s}^{nom}, C_{m,s}^{nom} \right) \longrightarrow \left(C_{lv,s}^{mod}, C_{m,s}^{mod} \right), \tag{I.12}$$

or

$$\left(C_{lv,s}^{mod}, C_{m,s}^{mod} \right) = \phi \left(\left(C_{lv,s}^{nom}, C_{m,s}^{nom} \right) \right). \tag{I.13}$$

For the details of the construction of $\phi(\cdot)$ see Appendix C.

I.7.3 Experimental data and theoretical signals

Let $\mathcal{A}$ be the set of all sensors with which the riser is instrumented. For every sensor $a \in \mathcal{A}$, let z_a^* be its (non-dimensional) location on the riser and let $(Y_{rms}^*)_{a,d}^{exp}$ denote the measured (non-dimensional) displacement rms

at that point. Furthermore, denote by $(Y^*_{rms})^{nom}_d = (Y^*_{rms})^{nom}_d(z)$ the nominal VIVA (non-dimensional) displacement rms signal. Note that all displacements (measured and VIVA-predicted) are indexed by d since they are different for different flow velocities and hence for different datacases.

By Equation (I.11), we may write

$$(Y^*_{rms})^{nom}_d = (Y^*_{rms})_d\left(z^*; C^{opt}_{lv,b}, C^{opt}_{m,b}, C^{nom}_{lv,s}, C^{nom}_{m,s}\right), d \in \mathcal{D}. \qquad (I.14)$$

A modified VIVA predicted signal $(Y^*_{rms})^{mod}_d$ corresponding to some transformation $\phi(\cdot)$ is given by

$$\begin{aligned}
(Y^*_{rms})^{mod}_d &= (Y^*_{rms})_d\left(z^*; C^{opt}_{lv,b}, C^{opt}_{m,b}, C^{mod}_{lv,s}, C^{mod}_{m,s}\right) \\
&= (Y^*_{rms})_d\left(z^*; C^{opt}_{lv,b}, C^{opt}_{m,b}, \phi\left(C^{nom}_{lv,s}, C^{nom}_{m,s}\right)\right), d \in \mathcal{D}. \qquad (I.15)
\end{aligned}$$

I.7.4   Objective function

The objective is to find the transformation $\phi(\cdot)$ that minimizes the overall deviation between theoretically predicted and experimentally observed response. More specifically, we wish to solve

$$\min_\phi \frac{1}{|\mathcal{D}||\mathcal{A}|} \sum_{d\in\mathcal{D}}\sum_{a\in\mathcal{A}} \left|(Y^*_{rms})_d\left(z^*_a; C^{opt}_{lv,b}, C^{opt}_{m,b}, \phi\left(C^{nom}_{lv,s}, C^{nom}_{m,s}\right)\right) - (Y^*_{rms})^{exp}_{a,d}\right|.$$
$$\qquad (I.16)$$

The transformation $\phi(\cdot)$ that achieves the minimum in Equation (I.16) is the optimal transformation and is denoted by $\phi^*(\cdot)$. The optimal straked databases are then given by

$$\left(C^{opt}_{lv,s}, C^{opt}_{m,s}\right) = \phi^*\left(\left(C^{nom}_{lv,s}, C^{nom}_{m,s}\right)\right), \qquad (I.17)$$

and the optimal VIVA predicted signals are

$$\begin{aligned}
(Y^*_{rms})^{opt}_d &= (Y^*_{rms})_d\left(z^*; C^{opt}_{lv,b}, C^{opt}_{m,b}, C^{opt}_{lv,s}, C^{opt}_{m,s}\right) \\
&= (Y^*_{rms})_d\left(z^*; C^{opt}_{lv,b}, C^{opt}_{m,b}, \phi^*\left(C^{nom}_{lv,s}, C^{nom}_{m,s}\right)\right), d \in \mathcal{D}. \qquad (I.18)
\end{aligned}$$

I.8   The optimization algorithm

In order to solve Equation (I.16) and thus find the optimal straked databases, we need an optimization algorithm. As explained in Appendix C, each transformation $\phi(\cdot)$ is essentially defined in terms of six scaling parameters and six translating parameters, a total of 12 parameters. Solving Equation (I.16) is then equivalent to minimizing a function over a 12-dimensional parameter space. Hence, an algorithm that works well in high dimensions is preferred. One such algorithm is the Nelder-Mead simplex method, presented by Nelder & Mead in 1965.

Thorough descriptions of the Nelder-Mead simplex method can be found in many papers, e.g. in the original Nelder & Mead (1965), or in Lagarias, et al. (1998). Appendix D briefly summarizes the method by outlining one iteration of the algorithm and explains how it is used to solve the problem at hand. We shall refrain from digging into the details of it in the main text. Note, however, that the Nelder-Mead simplex algorithm is an enormously popular direct search method (i.e. does not use derivative information to move from one iteration to another) for the minimization of multidimensional unconstrained problems. Its biggest caveat is perhaps the absence of established theoretical results (e.g. there are no provable convergence properties for general problem dimension), but in practice it has proved good enough for solving many problems in engineering, chemistry, biology, etc.

I.9   The results: optimal VIVA predictions and optimal databases

The results from the optimization are shown in Figures I.8 and I.9. Figure I.8 shows nominal and optimal VIVA-predicted displacement rms (continuous lines) against experimentally measured displacement rms at sensor locations (circles). Note that the optimal signals outperform the nominal ones in all cases, especially in the way they capture the decay in the straked region. As measured by our metric defined in Equation (I.16), the percentage reduction in error is approximately 30%. Figure I.9 shows how the VIVA-predicted peak response frequencies compare to the experimentally observed ones. Note the vast improvement that comes with the optimal databases, an error reduction
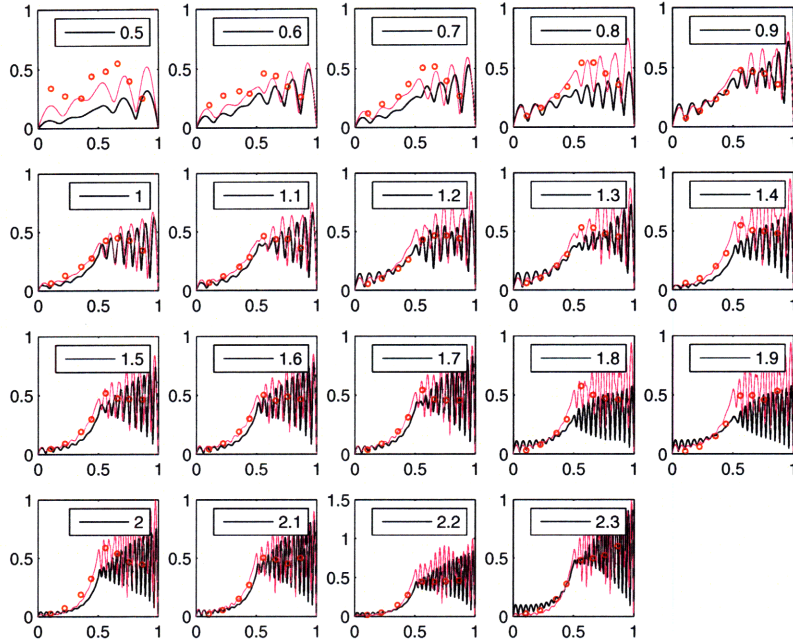
Figure I.8: Nominal (black) versus optimal (magenta) VIVA reconstructions. Abscissa is non-dimensional span, ordinate is non-dimensional displacement rms; label is flow velocity in m/s.
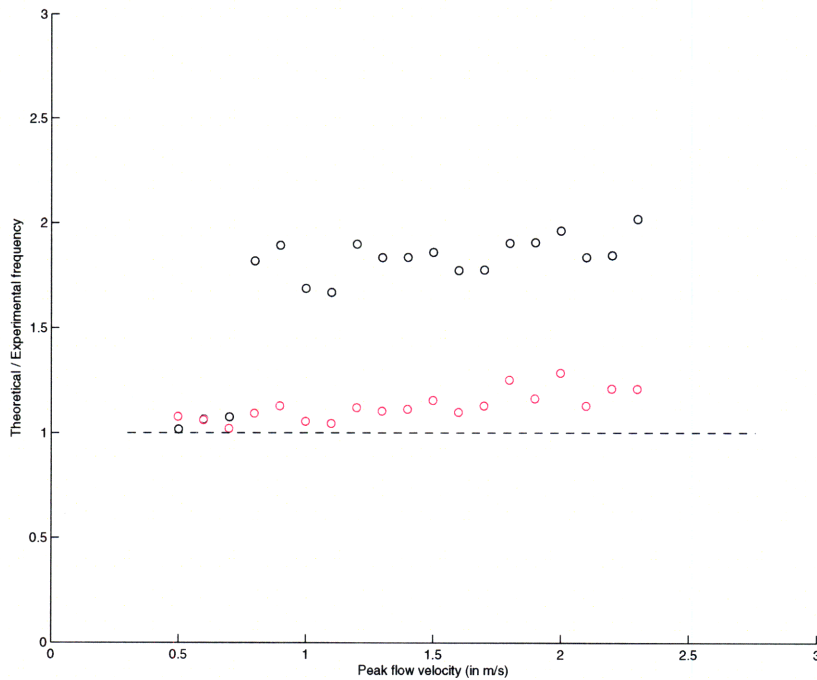
Figure I.9: Nominal (black) versus optimal (magenta) VIVA frequency comparisons.

of the order of 80%.

Finally, the optimal databases obtained are shown in Figures I.10-I.13. The major differences after optimization are the following. Firstly, the optimal C_{lv} falls slightly faster (both in Y^* and Vr) than the nominal one; this translates into a slightly sharper damping in the straked region, as seen in Figure I.8. Secondly (and most importantly), the C_m averages a much lower value in the optimal database (around 2.5) than in the nominal one (around 4.0); this, in turn, is responsible for the vast improvement in frequency prediction that is seen in Figure I.9.

I.10   Concluding remarks

In this first part of the thesis, we developed a systematic procedure that allowed us to use experimental data from real marine risers in order to correct force databases obtained in the laboratory. The methodology involved using the program VIVA and an optimization scheme: the force databases were modified through the optimization algorithm until the theoretical (VIVA-predicted) responses best matched the experimental (measured) data.

The results of Section 2.9 are quite encouraging; the errors in the the prediction of displacement and frequency were reduced by 30% and 80% respectively. Hence, confidence in the applicability of strip theory is established; furthermore, it is shown that warping transformations can be used to effectively account for Reynolds number and other real riser effects in VIV prediction.
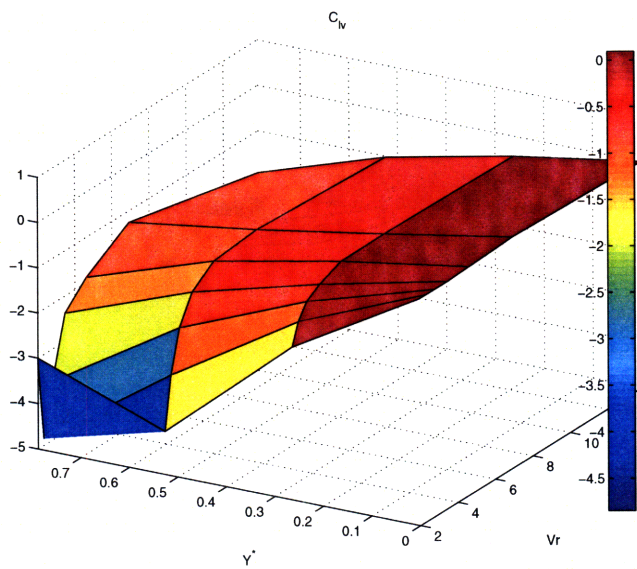
Figure I.10: Surface plot of optimal $C_{lv}(Vr, Y^*)$ database.
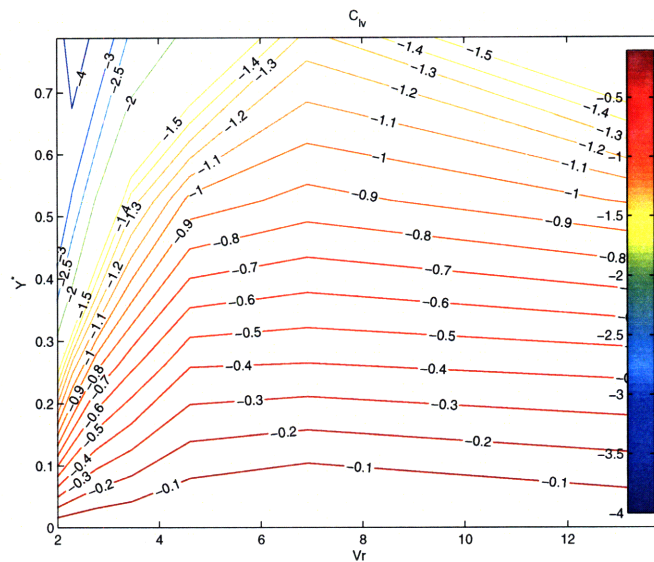
Figure I.11: Contour plot of optimal $C_{lv}(Vr, Y^*)$ database.
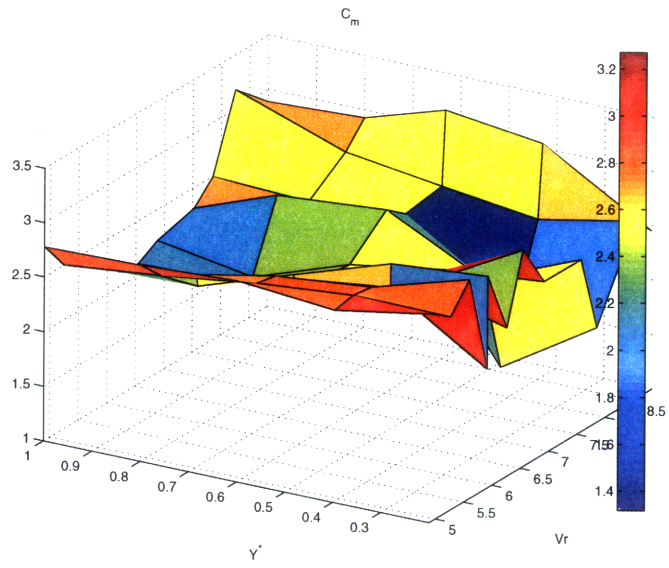
Figure I.12: Surface plot of optimal $C_m(Vr, Y^*)$ database.
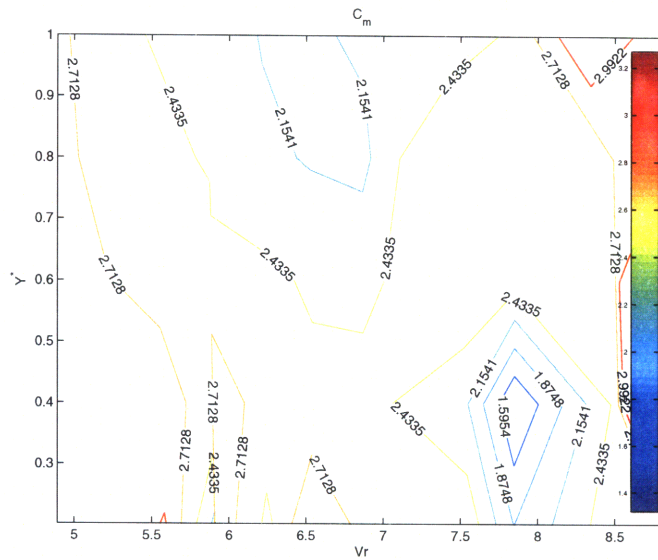
Figure I.13: Contour plot of optimal $C_m(Vr, Y^*)$ database.

Part II

Transient Response Analysis

II.1 Introduction

This part is on the transient response characteristics of riser VIV. Much research has gone into understanding and predicting steady-state vortex-induced motions of marine risers. Experimental observations, however, confirm that riser response may significantly change over time, even when external conditions (most importantly, the flow profile) remain unchanged. We wish to investigate the time-varying characteristics of risers undergoing VIV, and, for this purpose, we once again work with NDP experimental data. In particular, we examine datacases in the maximum flow velocity range $0.6m/s - 1.6m/s$ from the sheared bare, uniform bare, sheared straked and uniform straked datasets. We use the available sensor signals and statistical tools to conclude that the frequency content of the riser response may be either narrow-banded around a single dominant frequency (henceforth referred to as a Type I response) or distributed along a relatively broad range of frequencies (a Type II response). Transition from a Type I to a Type II response (and vice versa) can happen several times in a long enough time interval. Type I response means amplified 3rd harmonic displacement / acceleration / strain components, greater correlation length, organized riser motions and monochromatic travelling / standing waves. Type II response means smaller 3rd harmonic components, reduced correlation length, random-appearing riser motions and waves of several distinct frequencies. All datasets (sheared and uniform, bare and straked) exhibit responses of both types, al-

37
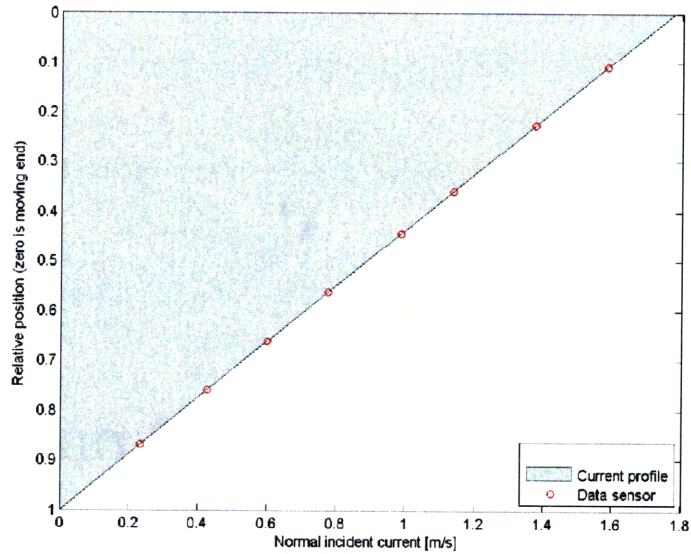
Figure II.1: Flow profile and sensor locations for NDP datacase 2460.

though there are some subtle differences between them. We close by identifying the regions on the riser that act as excitation sources (sheared datasets), and by finding an approximate range for the Strouhal numbers spanned by the excited frequencies (uniform datasets).

II.2 Transient response analysis of NDP datacase 2460

The purpose of this section is to walk through the analysis of datacase 2460 (maximum flow velocity of $1.7m/s$) from the sheared bare dataset. The velocity profile and accelerometer locations for this datacase are shown in Figure II.1.[1]

---

[1]The standing convention is that $z = 0$ is the moving end of the riser (the end of maximum flow velocity) for the sheared cases and the end where strakes start for the straked cases.

II.2.1 Transition and third harmonic

The time series plot and scalogram for accelerometer no. 4 (located more or less at the middle of the riser) are given in Figure II.2.[2] One can clearly distinguish the 1st and 3rd harmonics in the scalogram at about 8 and $24Hz$ respectively. One can also distinguish a jump in the 3rd harmonic near $4s$ and a fall again near $14s$.

To gain further insight, we plot a 3D version of the scalogram (Figure II.3). The mentioned jump and fall are now more apparent. We note that the change in the 3rd harmonic is more pronounced than the change in the 1st harmonic. Furthermore, the middle segment with the increased 3rd harmonic component (when compared with the segments that precede and follow it, which show reduced 3rd harmonic components) has a 1st harmonic component that is contained in a narrower frequency band. We identify the middle segment as a Type I segment, the segments immediately before and after it as Type II segments.

Finally, we plot the time series for accelerometer no. 4, first filtered around the 1st and then around the 3rd harmonic (Figure II.4). Again, we confirm the big jump and fall in the 1st and 3rd harmonics around 4 and $14s$ respectively.

We repeat for the remaining seven sensors and confirm that these observations hold along the length of the riser. Lastly, we check that the results hold not only for the acceleration signals, but also for the strain signals (see Figures II.5 and II.6). We conclude that:

> *A riser's response can show one of two types of behavior. When a riser shows (what we call) Type I behavior, the 1st harmonic component of the response tends to be confined within a narrow frequency band and the 3rd harmonic component is quite pronounced. On the other hand, when a riser shows Type II behavior, the spectrum is more spread out around the 1st harmonic and the 3rd harmonic in not as strong.*

---

[2]A scalogram is essentially a time-evolving spectrum obtained using wavelets.

39
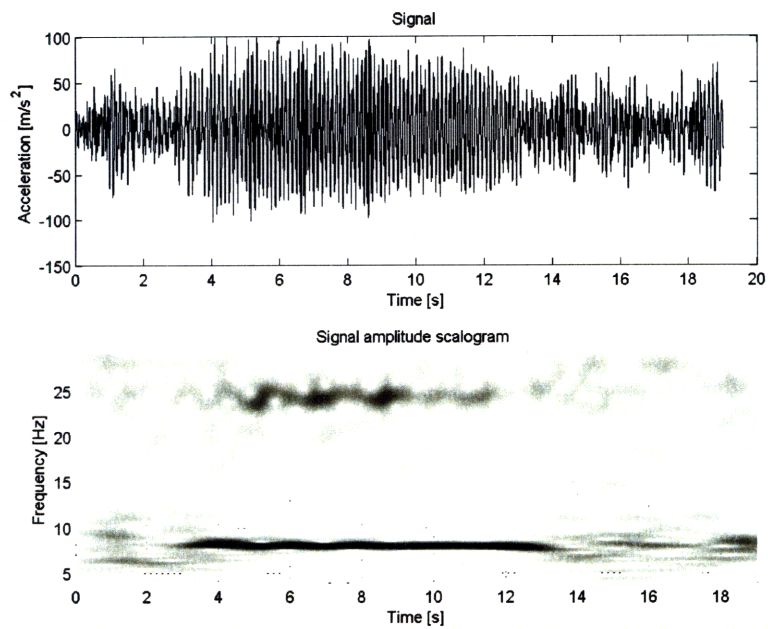
Figure II.2: Time series plot and scalogram for accelerometer no. 4.
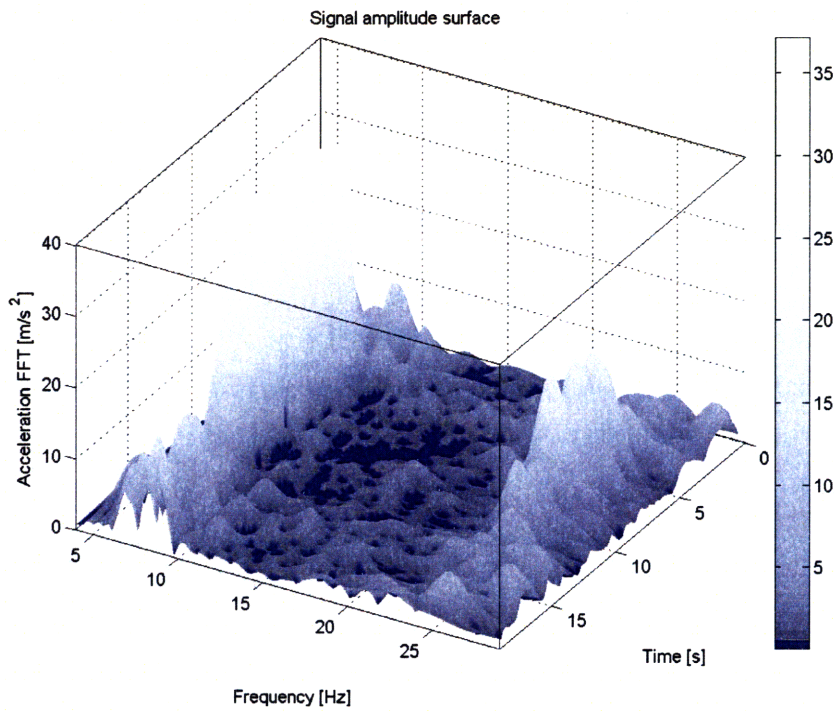
Figure II.3: 3D scalogram for accelerometer no. 4.
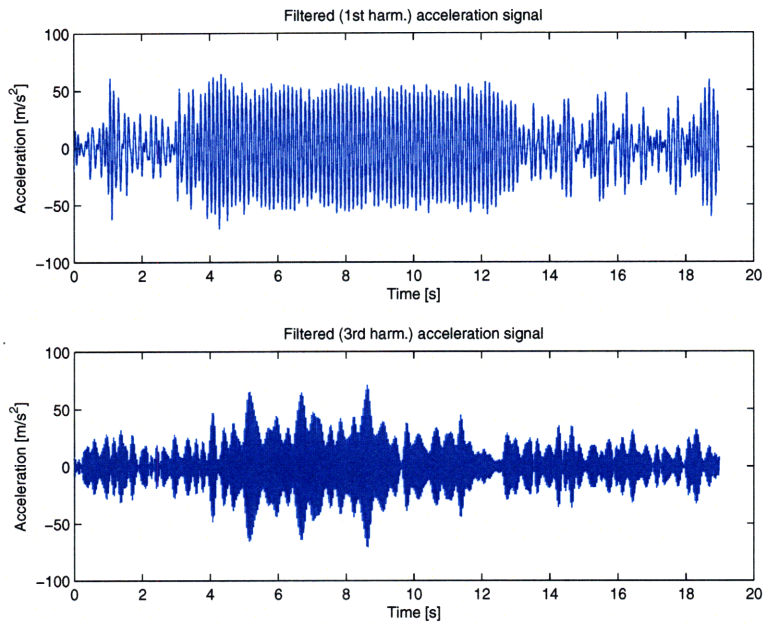
Figure II.4: 1st and 3rd harmonic time series plots for accelerometer no. 4.
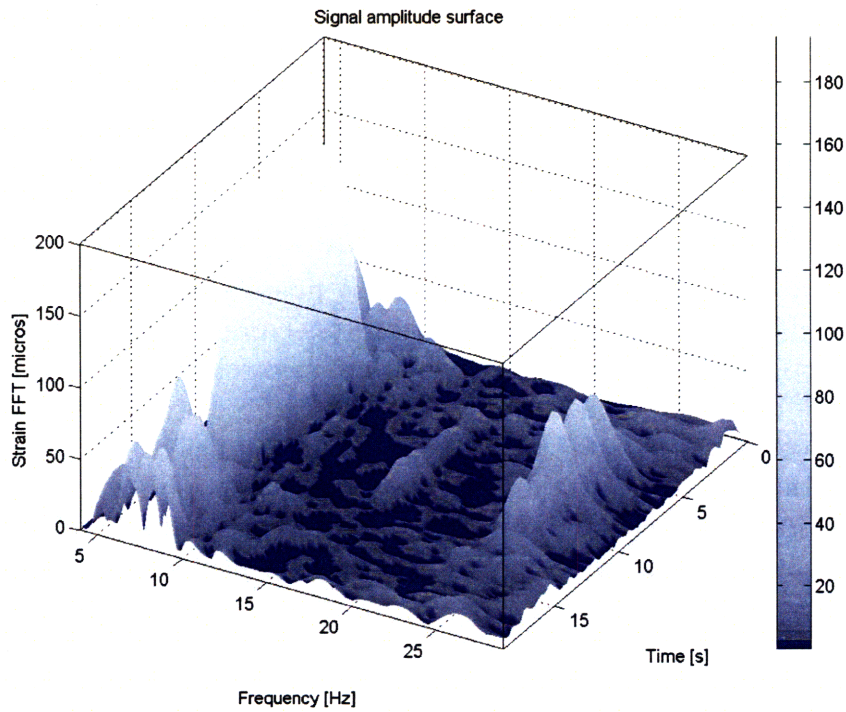
Figure II.5: 3D scalogram for the strain gauge nearest accelerometer no. 4.

41
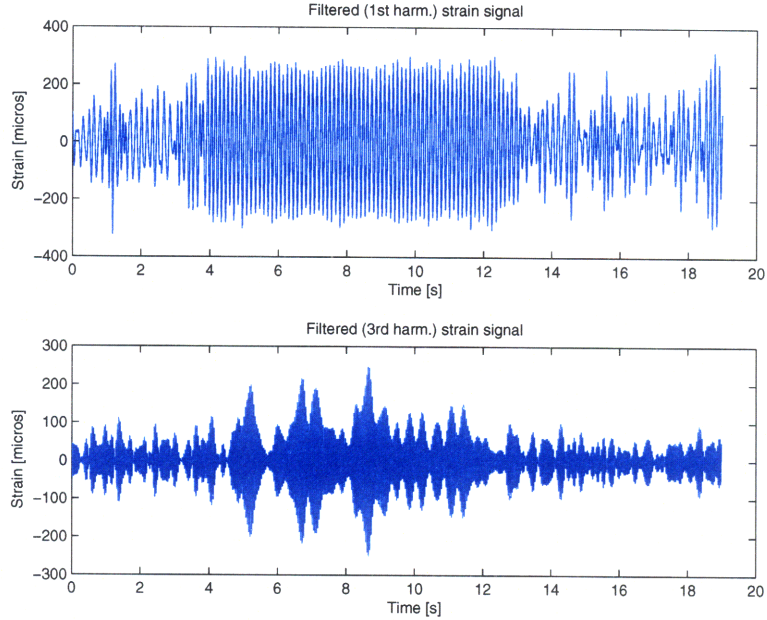
Figure II.6: 1st and 3rd harmonic time series plots for the strain gauge nearest accelerometer no. 4.

II.2.2 Transition and correlation length

Next, we investigate how the correlation length differs in Type I versus Type II events. In particular, we compute the maximum cross-correlations between all accelerometers for both types of events. [3]

The results are shown in Figure II.7. The figure shows cross-correlations between all eight sensors; black bars show cross-correlations during the Type I interval $5s - 12s$, while white bars show cross-correlations during the Type II interval $14s - 18s$. The first bar in the second cluster, for example, is the cross-correlation between sensors 2 and 3: the height of the black bar indicates that the cross-correlation between the two sensors during the Type I interval is around 0.61 and during the Type II interval around 0.49. It is evident that all sensors are significantly more correlated during the Type I

---

[3]The maximum cross-correlation between two signals, $y_1(t)$ and $y_2(t)$ is defined to be

$$\max_{\tau} \frac{\sum_t \left(y_1(t) - \overline{y_1}\right)\left(y_2(t - \tau) - \overline{y_2}\right)}{\sqrt{\sum_t \left(y_1(t) - \overline{y_1}\right)^2}\sqrt{\sum_t \left(y_2(t - \tau) - \overline{y_2}\right)^2}}, \tag{II.1}$$

where $\overline{y_1}$ and $\overline{y_2}$ are the means of y_1 and y_2 respectively.
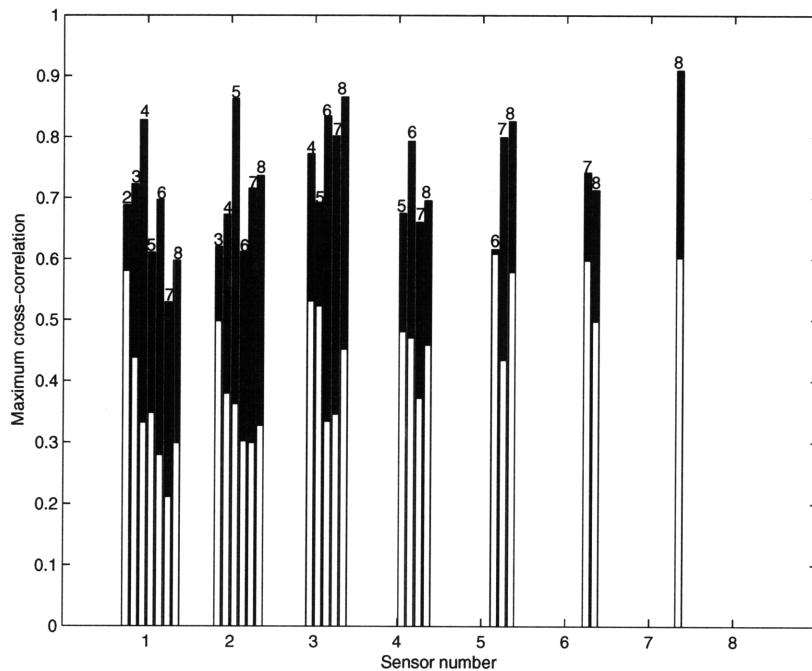
Figure II.7: Accelerometer cross-correlations during the Type I interval $5s - 12s$ (black) and the Type II interval $14s - 18s$ (white); note that black bars really extend all the way down to 0, but are partially covered by the white bars in front of them.

event.

We conclude that:

> *Type I events exhibit higher correlation lengths than Type II events (ceteris paribus).*

II.2.3 Transition and riser motion patterns

The riser's 'figure-8' motions (see Modarres-Sadeghi, et al. (2008)) are shown in Figure II.8. The figure should be read as follows. The abscissa is time in seconds. The ordinate is supposed to be indicative of the sensor's location on the $38m$ riser. The 'figure-8' shapes are filtered CF displacement versus filtered IL displacement (both filtered around the 1st harmonic). Only the

relative sizes of the 'figure-8' shapes are meaningful since they have been scaled (by the same factor) to fit in the figure. The color of the 'figure-8' is indicative of the phase difference between CF and IL, red meaning that CF significantly leads IL, blue that IL significantly leads CF and black that no motion significantly leads the other. We note that the 'figure-8' motions are very structured and well-organized during the Type I event $5s - 12s$, but random-looking during the Type II events that precede and follow. We conclude that:

> *During Type I events the riser's motions have neat 'figure-8' shapes; this is not the case for Type II events.*
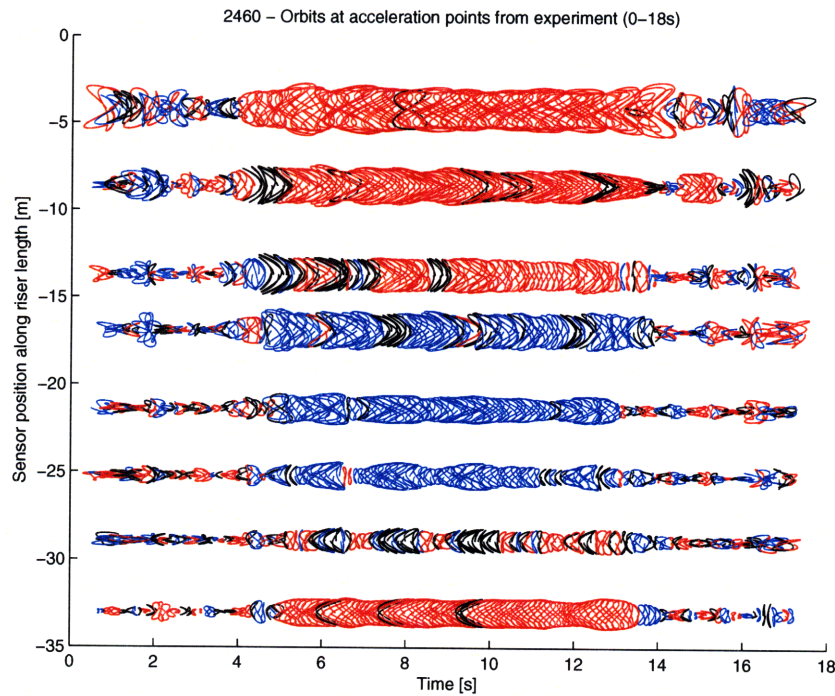
Figure II.8: Riser's 'figure-8' motions.

II.2.4   Transition and travelling waves

Up to this point, we have been looking directly at sensor signals. We refine our approach a bit and use the available signals to reconstruct the riser's mo-

tions. More specifically, we fit Fourier series to the experimentally measured points to obtain the displacement along the riser's span during the entire time history. The details are of no interest here and can be found in Mukundan (2008). The end-result is that we have at hand $y^*(z^*, t)$, non-dimensional CF displacement as a function of non-dimensional span and time.

We begin by simply plotting the reconstructed signal. A contour plot of $y^*(z^*, t)$ showing how the displacement nodes evolve in time is given in Figure II.9. The presence of clear, well-organized travelling waves originating from the higher velocity end is evident in the Type I interval $5s - 12s$. The Type II intervals before and after are more disordered and show no obvious pattern.
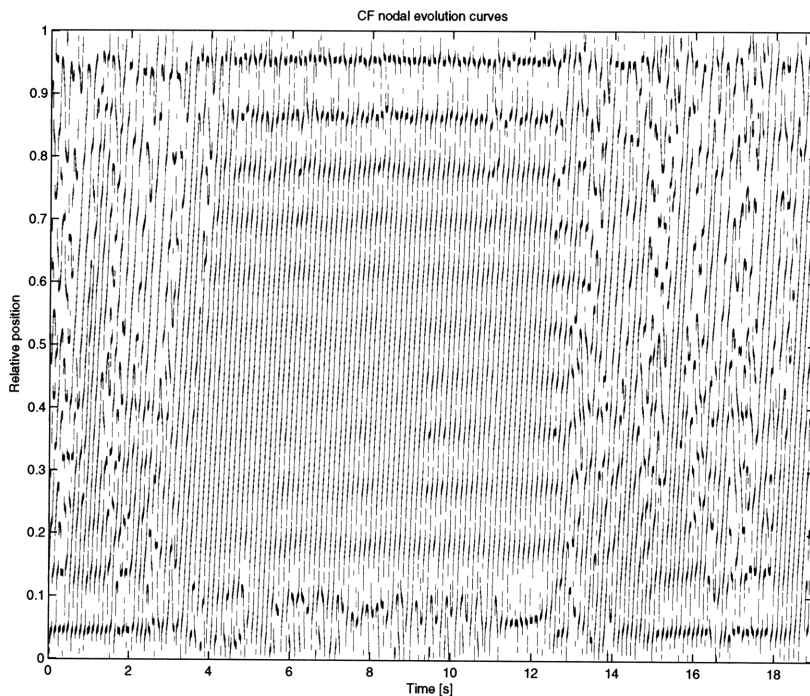
Figure II.9: Nodal evolution curves.

We proceed to take a double Fourier transform (in space and time) of $y^*(z^*, t)$ in order to see if (and how) the picture in the frequency domain changes when we leave a Type II event and enter a Type I event (and vice versa). First, we recall that if $y^*(z^*, t)$ is of the form

$$y^*(z^*, t) = \sin(k_0 z^*) \sin(\omega_0 t) \qquad \text{(II.2)}$$

45
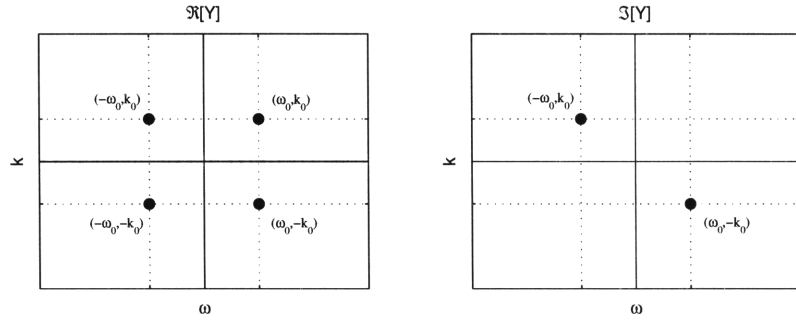
Figure II.10: 2D Fourier transforms for pure standing (left) and pure travelling (right) waves.

(a pure standing wave), then the double Fourier transform is given by

$$Y(k,\omega) \equiv \frac{1}{\pi^2} \int\int y^*(z^*,t) e^{-i(kz^*+\omega t)} dz^* dt$$
$$= \delta(\omega + \omega_0)\delta(k + k_0) + \delta(\omega + \omega_0)\delta(k - k_0)$$
$$+ \delta(\omega - \omega_0)\delta(k + k_0) + \delta(\omega - \omega_0)\delta(k - k_0), \qquad \text{(II.3)}$$

where $\delta(\cdot)$ is the Dirac delta function. Similarly, if $y^*(z^*,t)$ is of the form

$$y^*(z^*,t) = \sin(k_0 z^* - \omega_0 t) \qquad \text{(II.4)}$$

(a pure travelling wave), then the double Fourier transform is given by

$$Y(k,\omega) = 2i\left[\delta(\omega - \omega_0)\delta(k + k_0) - \delta(\omega + \omega_0)\delta(k - k_0)\right]. \qquad \text{(II.5)}$$

The spectra given in Equations (II.3) and (II.5) have been plotted in Figure II.10.

We proceed to take a double Fourier transform of the reconstructed displacement signal $y^*(z^*,t)$ for the Type I interval $5s - 12s$ as well as for the Type II intervals that precede and follow it. The results are shown in Figures II.11, II.12 and II.13. Note that instead of $Y(k,\omega)$ we plot the more convenient $Y(k, f = \omega/2\pi)$.

There are two important observations to make here. The Type I event shows one single peak in the spectrum and no significant standing wave components

46
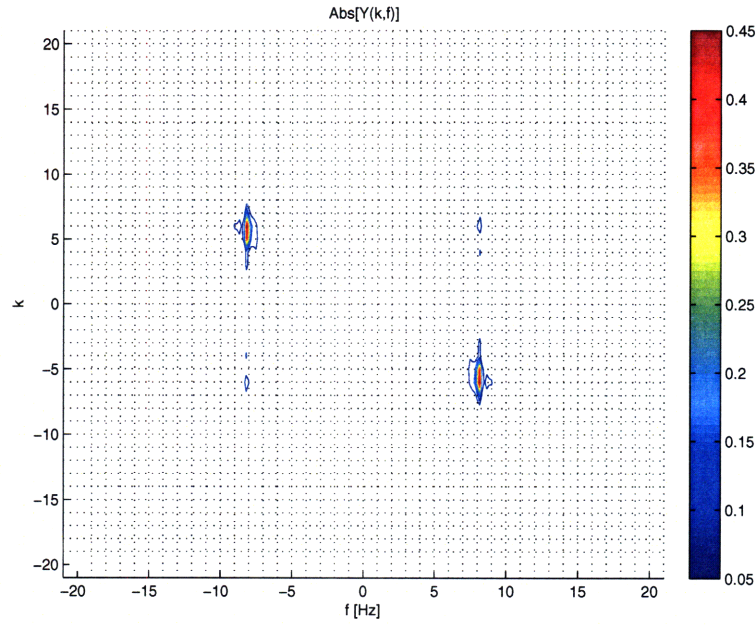
Figure II.11: 2D spectrum $Y(k, f)$ of the reconstructed displacement signal $y^*(z^*, t)$ for the Type I interval $5s - 12s$.
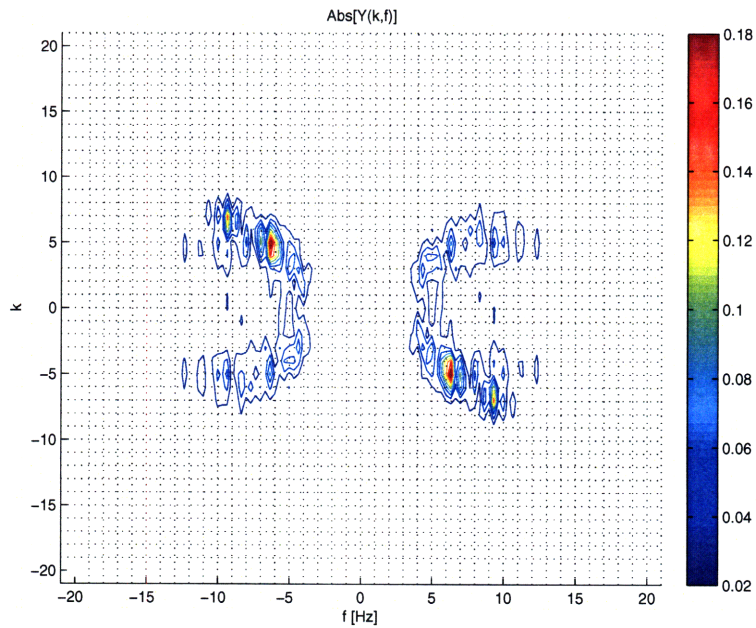
Figure II.12: 2D spectrum $Y(k, f)$ of the reconstructed displacement signal $y^*(z^*, t)$ for the Type II interval $0s - 3s$.
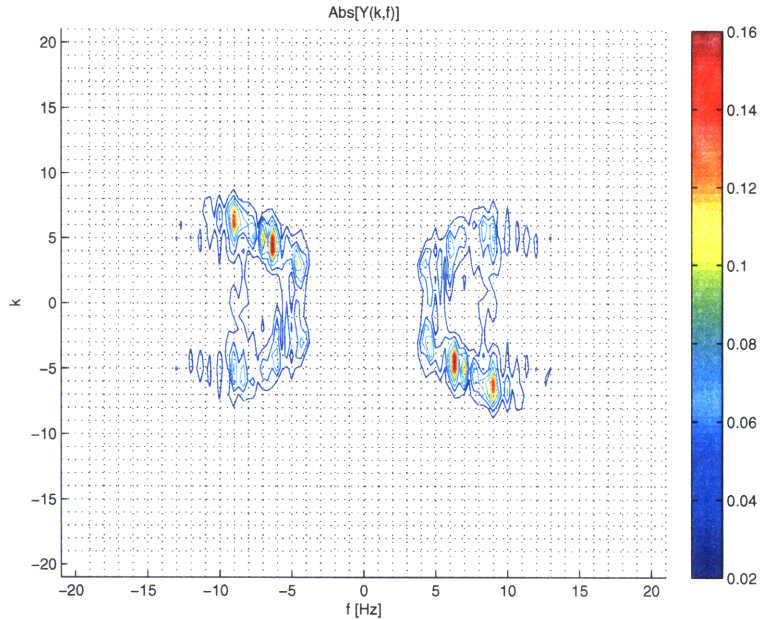
Figure II.13: 2D spectrum $Y(k, f)$ of the reconstructed displacement signal $y^*(z^*, t)$ for the Type II interval $14s - 18s$.

(all peaks live in the second and fourth quadrants). On the other hand, the Type II events show several distinct peaks in the spectrum, with significant travelling and standing wave components. We conclude that:

Type I events show one single peak in the 2D displacement spectrum and no significant standing wave components, whereas Type II events show multiple peaks in the 2D displacement spectrum, with significant travelling and standing wave components.

II.3 Transient response analysis of other NDP datacases

Section 3.2 introduced various tools for the analysis of the transient response of marine risers by considering datacase 2460 from the NDP experiments. This section attempts to summarize the conclusions reached by applying these tools to other NDP datasets (uniform and sheared, bare and straked). In short, the observations on the 3rd harmonic, the correlation length and the riser's orbits hold more or less unchanged throughout the cases. However,

the various datasets do differ a bit when it comes to travelling waves. A comprehensive list of conclusions follows.

1. Type I intervals (when compared to Type II intervals) show relatively narrow-banded 1st harmonic and strengthened 3rd harmonic responses.

2. Type I intervals (when compared to Type II intervals) exhibit higher correlation lengths.

3. During Type I intervals, the riser's motions have clear 'figure-8' shapes; this does not hold during Type II intervals.

4. Type I events often show one single peak in the 2D displacement spectrum and no significant standing wave components; Type II spectra tend to be more spread out, often with multiple peaks and significant travelling and standing wave components.

5. The sheared bare cases show travelling waves always originating from the higher velocity end. However, some cases primarily show monochromatic response (and hence are mainly characterized by Type I events), while other cases primarily show multi-frequency response (and hence are dominated by Type II events).

6. The uniform bare cases show both left and right travelling waves. They also show significant standing wave components in many cases. Almost all cases show multiple excited frequencies, but these are contained within tighter frequency bands compared to the sheared bare cases.

7. The straked cases show travelling waves always originating from the bare end, and also show significant standing wave components in many cases. The sheared straked cases have excited frequencies in much wider frequency ranges than the uniform straked cases.

II.4 From excited frequencies to riser excitation regions

For the sheared NDP cases, we take one step further. For each datacase, we use the obtained peak frequencies together with the Strouhal relation,

$$\frac{fD}{z^*U_{max}} = St \approx 0.17, \qquad (II.6)$$

in order to identify the riser excitation regions.

The results are shown in Figures II.14 and II.15. Each subplot has non-dimensional span as its abscissa. The lobes are the significant peaks seen in the frequency spectrum, each lobe having a height equal to its height in the spectrum. We observe that:

> *For the sheared bare cases only the higher velocity half acts as a source of excitation, the most powerful exciting region being the one extending from $z^* \approx 0.1$ to $z^* \approx 0.3$. Similarly, for the sheared straked cases only the bare part acts as a source of excitation, most of the excitation coming from $z^* \approx 0.6$ to $z^* \approx 0.8$.*

II.5 Strouhal range spanned by excited frequencies

For each datacase from the uniform NDP cases, we use the obtained peak frequencies together with the Strouhal relation,

$$St = \frac{fD}{U_{max}}, \qquad (II.7)$$

in order to identify the Strouhal range spanned by the excited frequencies.

The results are shown in Figures II.16 and II.17. Each subplot has Strouhal number as its abscissa, and again the lobes are the significant peaks seen

50
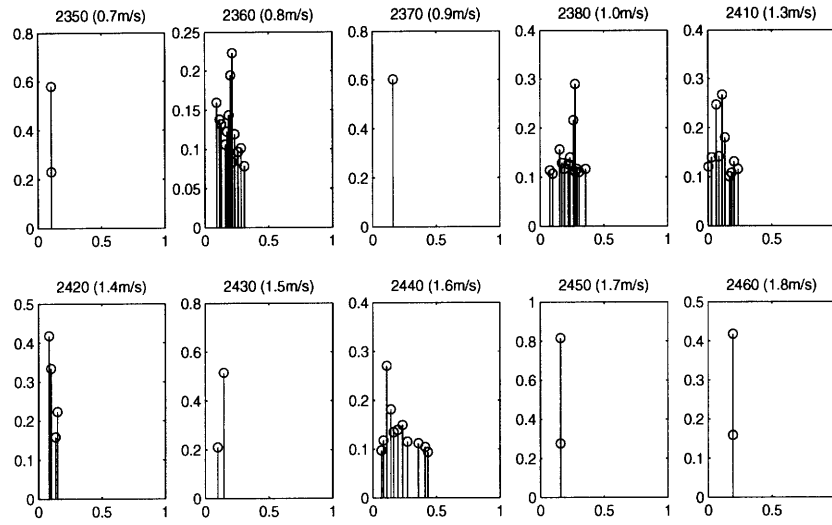
Figure II.14: Excitation regions for the sheared bare NDP experiments.
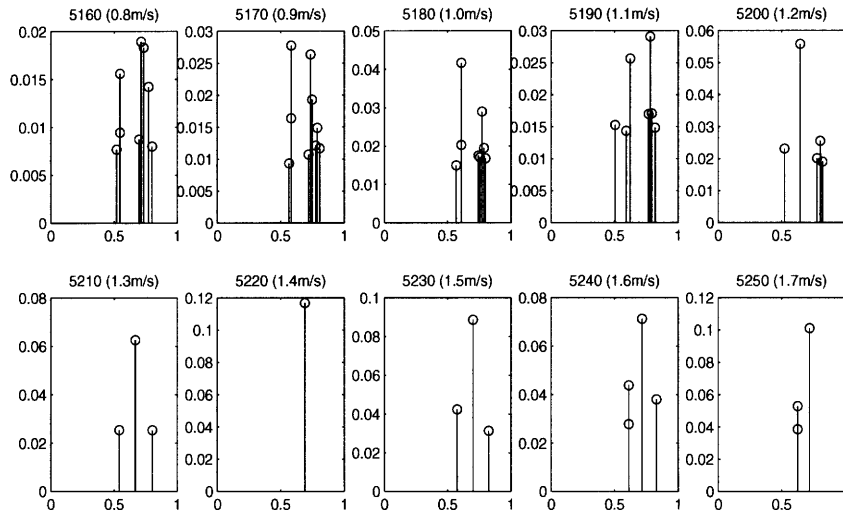
Figure II.15: Excitation regions for the sheared straked NDP experiments.

in the 2D spectrum (each lobe having a height equal to its height in the spectrum). We note that:

> *The Strouhal range spanned by the excited frequencies is approximately* 0.13 − 0.17.

II.6   Concluding remarks

This second part of the thesis showed the existence of two distinct types of riser response, one narrow-banded around a single frequency (termed a Type I response) and another extending over several frequencies (a Type II response). We showed that Type I (relative to Type II) responses show strong higher harmonic components, organized riser motions, and monochromatic travelling waves (originating from the higher velocity end in sheared currents and from the bare part in straked risers). We also showed that the Strouhal range spanned by the excited frequencies is 0.13−0.17 (with a median value of 0.15), this range being broader for sheared (as opposed to uniform) currents.

The work on transient response presented herein is at its very early stages; there are significant aspects of the topic that need to be further examined. Probably the most interesting question left unanswered is what exactly causes the transition from a Type I to a Type II response (and vice versa), especially given that external conditions remain unchanged.
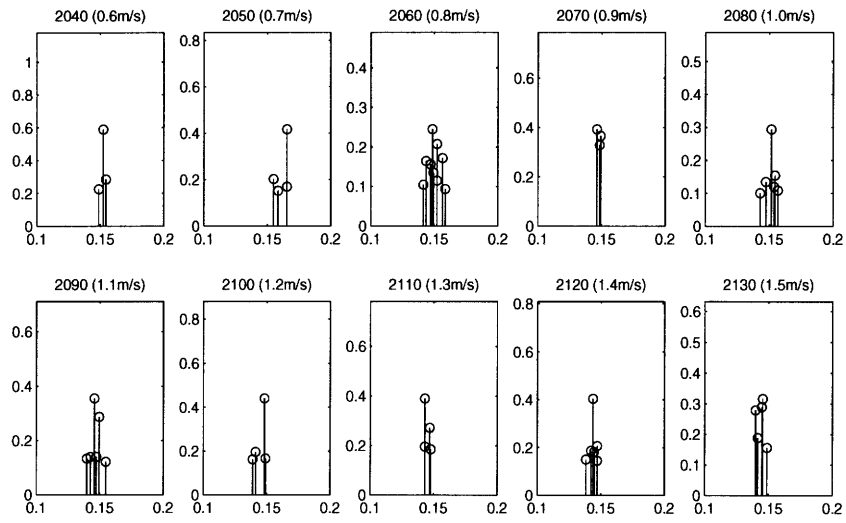
Figure II.16: Strouhal ranges spanned by the uniform bare NDP experiments.
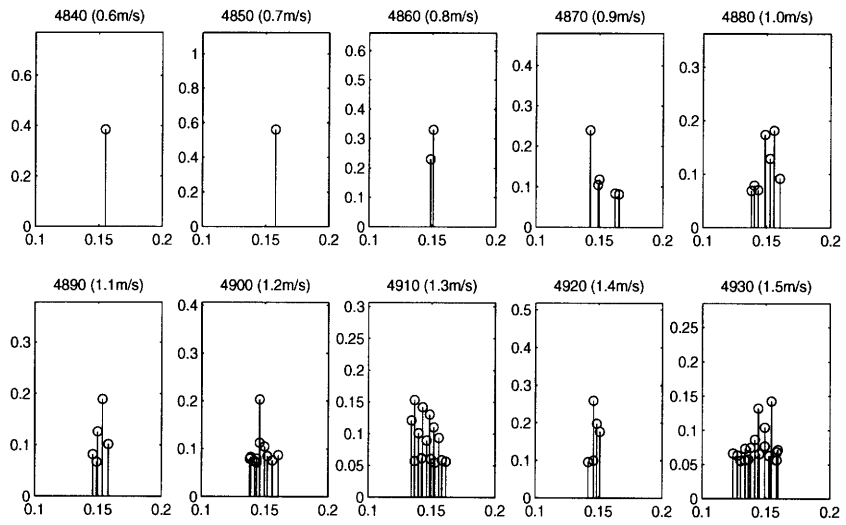
Figure II.17: Strouhal ranges spanned by the uniform straked NDP experiments.

Bibliography

[1] Bearman. (1984). Vortex shedding from oscillating bluff bodies. *Annual review of fluid mechanics , 16,* 195-222.

[2] Bertsekas, D. (2008). *Introduction to probability* (2nd ed.). Athena Scientific.

[3] Blevins, R. (1990). *Flow induced vibrations* (2nd ed.). New York, NY: Van Nostrand Reinhold.

[4] Bliek, A. (1984). *Dynamic analysis of single span cables (Ph.D. thesis).* Cambridge, MA: Massachusetts Institute of Technology.

[5] Boyce, W., & DiPrima, R. (2004). *Elementary differential equations and boundary value problems* (8th ed.). Wiley.

[6] Braaten, H., & Lie, H. (2004). *NDP riser high mode VIV tests main report.* Norwegian Marine Technology Research Institute.

[7] Byatt, D. (2000). *Convergent variants of the Nelder-Mead algorithm (Masters thesis).* Christchurch, New Zealand: University of Canterbury.

[8] Carmona, R. (2004). *Statistical analysis of financial data in S-Plus.* New York: Springer.

[9] Dahl, J. (2008). *Vortex induced vibrations of a circular cylinder with combined in-line and cross-flow motions (Ph.D. thesis).* Cambridge, MA: Massachusetts Institute of Technology.

[10] Dahl, J., Hover, F., Triantafyllou, M., Dong, S., & Karniadakis, G. (2007). The singular effect of multi-vortex patterns on the fatigue life of ocean structures. *Physical review letters, 99.*

[11] Devore, J. (2003). *Probability and statistics for engineering and the sciences* (6th ed.). Duxbury Press.

[12] Ding, Z., Balasubramanian, S., Lokken, R., & Yung, T. (2004). Lift and damping characteristics of bare and straked cylinders at riser scale Reynolds numbers. Houston.

[13] Gopalkrishnan, R. (1993). *Vortex-induced forces on oscillating bluff cylinders (Ph.D. thesis)*. Cambridge, MA: Massachusetts Institute of Technology.

[14] Govardan, R., & Williamson, C. (2006). Defining the modified Griffin plot in vortex-induced vibration: revealing the effect of Reynolds number using controlled damping. *Journal of fluid mechanics , 561,* 147-180.

[15] Graff, K. (1991). *Wave motion in elastic solids.* New York, NY: Dover.

[16] Grinfogel, L. (1984). *Dynamics of elastic taut inclined cables (Masters thesis)*. Cambridge, MA: Massachusetts Institute of Technology.

[17] Hildebrand, F. (1976). *Advanced calculus for applications* (2nd ed.). Prentice Hall.

[18] Howell, C., & Triantafyllou, M. (1993). Stable and unstable nonlinear resonant response of hanging chains: theory and experiment. *Proceedings: mathematical and physical sciences. 440,* pp. 345-364. The Royal Society of London.

[19] Irvine, H., & Caughey, T. (1974). The linear theory of free vibrations of a suspended cable. *Proceedings: mathematical and physical sciences. 341,* pp. 299-315. The Royal Society of London.

[20] Kelley, C. (2000). Detection and remediation of stagnation in the Nelder-Mead algorithm using a sufficient decrease condition. *SIAM journal on optimization, 10,* 43-55.

[21] Kristansen, L., & Lie, H. (2005). *NDP riser high mode VIV tests: response analysis*. Trondheim: MARINTEK.

[22] Lagarias, J., Reeds, J., Wright, H., & Wright, P. (1998). Convergence properties of the Nelder-Mead simplex method in low dimensions. *SIAM journal on optimization, 9,* 112-147.

[23] Marcollo, H., & Hinwood, J. (2006). On shear flow single mode lock-in with both cross-flow and in-line lock-in mechanisms. *Journal of fluids and structures, 22,* 197-211.

[24] Marsden, J., & Tromba, A. (2003). *Vector calculus* (5th ed.). W.H. Freeman.

[25] McKinnon, K. (1998). Convergence of the Nelder-Mead simplex method to a non-stationary point. *SIAM journal on optimization, 9,* 148-158.

[26] Modarres-Sadeghi, Y., Triantafyllou, M., & Hover, F. (2008). Fatigue life calculations of risers taking into account the higher-harmonic force components. *Proceedings of the 18th international offshore and polar engineering conference.* Vancouver.

[27] Mukundan, H. (2008). *Vortex-induced vibrations of marine risers: motion and force reconstruction from field and experimental data (Ph.D. thesis).* Camridge, MA: Massachusetts Institute of Technology.

[28] Nelder, J., & Mead, R. (1965). A simplex method for function minimization. *Computer Journal, 7,* 308-313.

[29] Newman, J. (1977). *Marine hydrodynamics.* Cambridge, MA: The MIT press.

[30] Pantazopoulos, M. (1994). Vortex-induced vibration parameters: a critical review. *ASME. I.* OMAE.

[31] Ross, S. (2000). *Introduction to probability models* (7th ed.). Academic Press.

[32] Routh, E. (1955). *Dynamics of a system of rigid bodies.* New York, NY: Dover.

[33] Sarpkaya, T. (2004). A critical review of the intrinsic nature of vortex-induced vibrations. *Journal of fluids and structures , 19,* 389-447.

[34] Sarpkaya, T. (1995). Hydrodynamic damping, flow-induced oscillations and biharmonic response. *Journal of offshore mechanics and arctic engineering , 117,* 232-238.

[35] Smogeli, O., Hover, F., & Triantafyllou, M. (2003). Force feedback control in VIV experiments. *22nd international conference on offshore mechanics and arctic engineering.* Cancun.

[36] Triantafyllou, G. (1998). Vortex induced vibrations of long cylindrical structures. *Summer meeting of the American Society of Mechanical Engineers (ASME).* Washington, D.C.

[37] Triantafyllou, M. (1987). Dynamics of cables and chains. *The shock and vibration digest, 19,* 3-5.

[38] Triantafyllou, M. (1984). The dynamics of taut inclined cables. *Journal of mechanics and applied mathematics, 37.*

[39] Triantafyllou, M. (2006). *VIVA: Programs for calculating riser vortex induced oscillations and fatigue life.* MIT, Cambridge.

[40] Triantafyllou, M., Triantafyllou, G., Tein, Y., & Ambrose, B. (1999). Pragmatic riser VIV analysis. *Offshore technology conference.* Houston.

[41] Trim, A., Braaten, H., Lie, H., & Tognarelli, M. (2005). Experimental investigation of vortex-induced vibrations of long marine risers. *Journal of fluids and structures, 21,* 335-361.

[42] Vandiver, J. (1993). Dimensionless parameters important to the prediction of vortex-induced vibrations of long, flexible cylinders in ocean currents. *Journal of fluids and structures, 7,* 423-455.

[43] von Karman, T., & Biot, M. (1944). *Mathematical methods in engineering.* McGraw Hill.

[44] Williamson, C., & Govardan, R. (2004). Vortex-induced vibrations. *Annual review of fluid mechanics , 36,* 413-455.

[45] Williamson, C., & Jauvtis, N. (2004). A high amplitude 2T mode of vortex-induced vibration for a light body in XY motion. *European journal of mechanics of fluids , 23,* 107-114.

Appendix A

Experimental Data

Almost all of the work in this thesis uses data from high-mode VIV experiments conducted by the Norwegian Deepwater Programme (NDP) in 2003. Detailed descriptions of the experimental setup can be found in Kristansen & Lie (2005) and Trim, et al. (2005). A brief summary follows.

The tests were conducted at Marintek's ocean basin in Trondheim and involved towing a long fiberglass riser through the basin. The experiment used a bare riser model as a base case (see Table A.1 for basic model properties). First both ends of the riser were towed simultaneously at the same velocity, thus achieving a uniform flow velocity profile; then one end of the riser was kept at rest while the other end was made to follow a predefined circular arc, thus achieving a sheared velocity profile. The same procedure was repeated for different tow speeds and for straked risers of different strake coverage percentages (see Table A.2 for basic strake properties). The tests of interest to this thesis are summarized in Tables A.3-A.4.

Property	Dimension
Total length between pinned ends (m)	38
Outer diameter (m)	0.027
Wall thickness (m)	0.003
Young's modulus (N/m^2)	2.25E+09
Bending stiffness (Nm^2)	37.2
Mass per unit length, air-filled (kg/m)	0.761
Mass per unit length, water-filled (kg/m)	0.933
Tension (N)	5000 (approx.)

Table A.1: Basic NDP riser properties.

Property	Dimension
Outer sleeve diameter (m)	0.032
Pitch / Diameter	17.5
Height / Diameter	0.25
Weight in water (N/m)	2.79

Table A.2: Basic NDP strake properties.
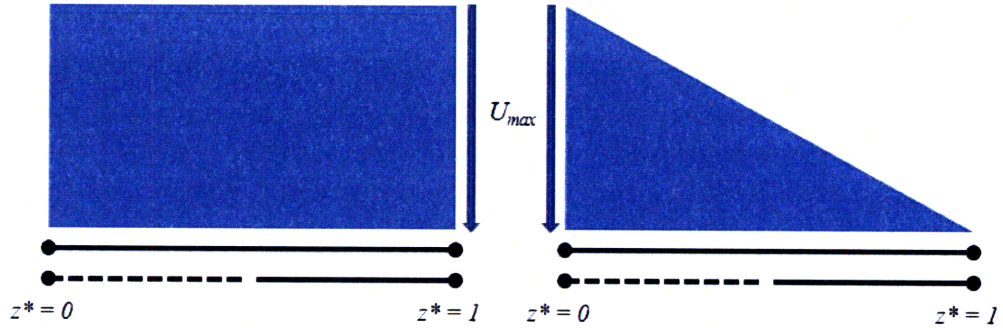
Figure A.1: Riser configuration and flow distribution for NDP experiments; left: uniform flow velocity profile, right: sheared profile. Note the conventions used throughout the thesis: whenever strakes are present, they start at the $z^* = 0$ end; whenever there is a flow velocity gradient, the $z^* = 0$ end is the end of highest velocity.

	U_{max} (m/s)	Uniform Datacase no.	Sheared Datacase no.
Bare	0.3	2010	2310
	0.4	2020	2320
	0.5	2030	2330
	0.6	2040	2340
	0.7	2050	2350
	0.8	2060	2360
	0.9	2070	2370
	1.0	2080	2380
	1.1	2090	2390
	1.2	2100	2400
	1.3	2110	2410
	1.4	2120	2420
	1.5	2130	2430
	1.6	2140	2440
	1.7	2150	2450
	1.8	2160	2460
	1.9	2170	2470
	2.0	2180	2480
	2.1	2190	2490
	2.2	2200	2500
	2.3	2210	2510
	2.4	2220	2520

Table A.3: NDP bare tests.

	U_{max} (m/s)	Uniform Datacase no.	Sheared Datacase no.
Straked (50%)	0.3	4810	5110
	0.4	4820	5120
	0.5	4830	5130
	0.6	4840	5140
	0.7	4850	5150
	0.8	4860	5160
	0.9	4870	5170
	1.0	4880	5180
	1.1	4890	5190
	1.2	4900	5200
	1.3	4910	5210
	1.4	4920	5220
	1.5	4930	5230
	1.6	4940	5240
	1.7	4950	5250
	1.8	4960	5260
	1.9	4970	5270
	2.0	4980	5280
	2.1	4990	5290
	2.2	5000	5300
	2.3	5010	5310
	2.4	5020	5320

Table A.4: NDP straked tests.

Appendix B

A Heuristic Procedure for Obtaining Reliable Bare Databases

Mukundan (2008) presented a systematic procedure for obtaining optimal force databases for bare marine risers. The procedure relied on parameterizing the bare $C_{lv}\left(Vr, Y^*\right)$ and $C_m\left(Vr, Y^*\right)$ surfaces (the ones presented in Figures I.2 and I.3) and then using an optimization algorithm to cleverly modify the chosen parameters until good agreement with experimental data was achieved (as measured by an appropriately defined error metric). The method we present here is an alternative to the one proposed by Mukundan. It is less general, since it can only be used with the program VIVA and involves a lot of non-automated work; however, the results it gives for a wide range of data are very good.

VIVA (see Triantafyllou (2006)) uses C_{lv} and C_m data in a specific format; the following need to be provided in an input file:

1. $\mathbb{V}$, a set of non-dimensional velocities (Vr) (or frequencies $(1/Vr)$) in the range of interest,

2. $C_{lv}\left(Vr, Y^* = 0\right), \forall Vr \in \mathbb{V}$,

3. $C_m\left(Vr, Y^* = 0\right), \forall Vr \in \mathbb{V}$,

4. $Y_0^*(Vr)$, the value of Y^* where $C_{lv}(Vr, Y^*)$ attains its maximum for any given $Vr \in \mathbb{V}$,

5. $s_1(Vr)$, an average value of the slope of $C_{lv}(Vr, Y^* < Y_0^*(Vr))$ for any given $Vr \in \mathbb{V}$, and finally

6. $s_2(Vr)$, an average value of the slope of $C_{lv}(Vr, Y^* > Y_0^*(Vr))$ for any given $Vr \in \mathbb{V}$.

Being guided by the form of the force databases for rigid cylinders and the available experimental observations for real-scale marine risers, we are lead to consider simple forms for $C_{lv}(Vr, 0)$, $C_m(Vr, 0)$, $Y_0^*(Vr)$, $s_1(Vr)$, and $s_2(Vr)$, like the ones given in Figure B.1 on the next page. We subsequently parameterize the forms (as shown) and systematically modify the parameters, testing each parameter set for the quality of predictions it gives (this procedure involves a fair amount of trial and error).

For the purposes of this thesis, it was natural to test each set of parameters for its predictions on bare, sheared NDP data. The following parameter values gave good predictions:

$$(f_0, f_1, f_2, f_3, f_4, f_5, f_6, f_7, f_8, c_1, c_2, c_3, c_4, s_1, s_2, a_0) =$$

$$(0.14, 0.10, 0.17, 0.20, 0.26, 0.30, 0.34, 0.44, 0.50, 0.35, 0.60, 0.70, 1.15, 1.0, 2.0, 0.35).$$

Figures B.2 and B.3 compare VIVA predictions under the nominal bare databases and the ones corresponding to the parameter values listed above.
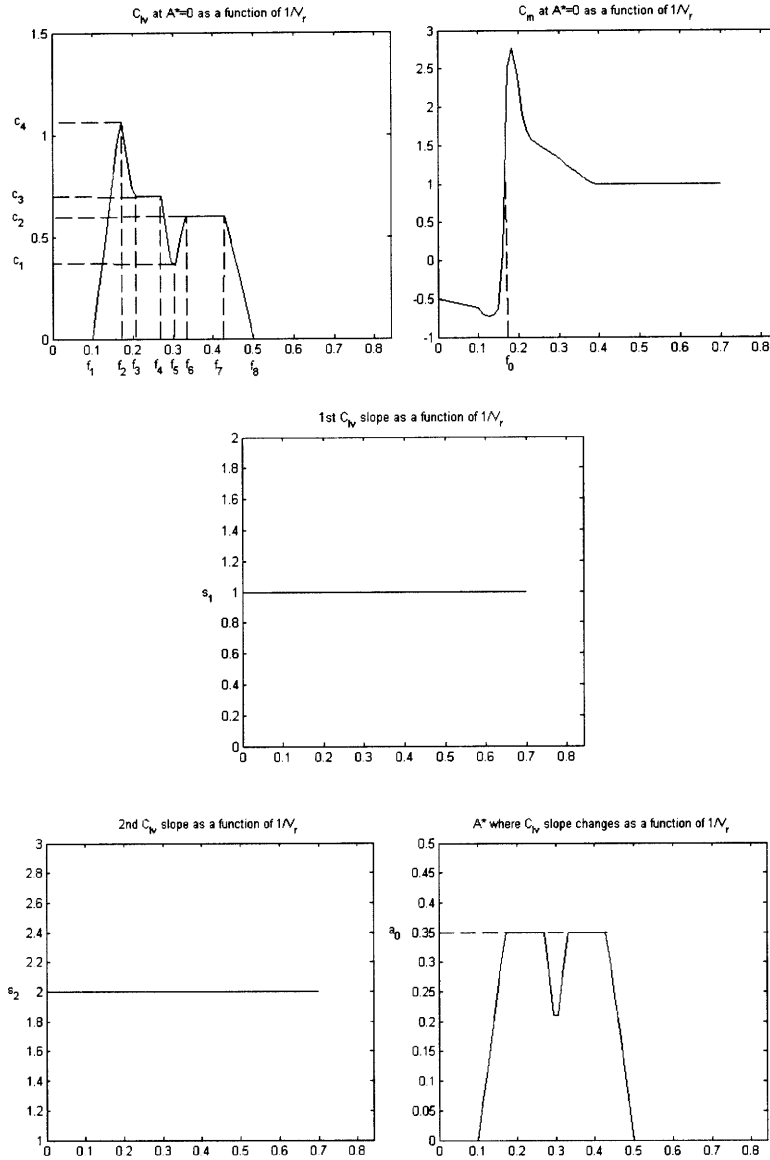
Figure B.1: Parameterization of the bare force databases; abscissa is $1/Vr$ for all subplots.
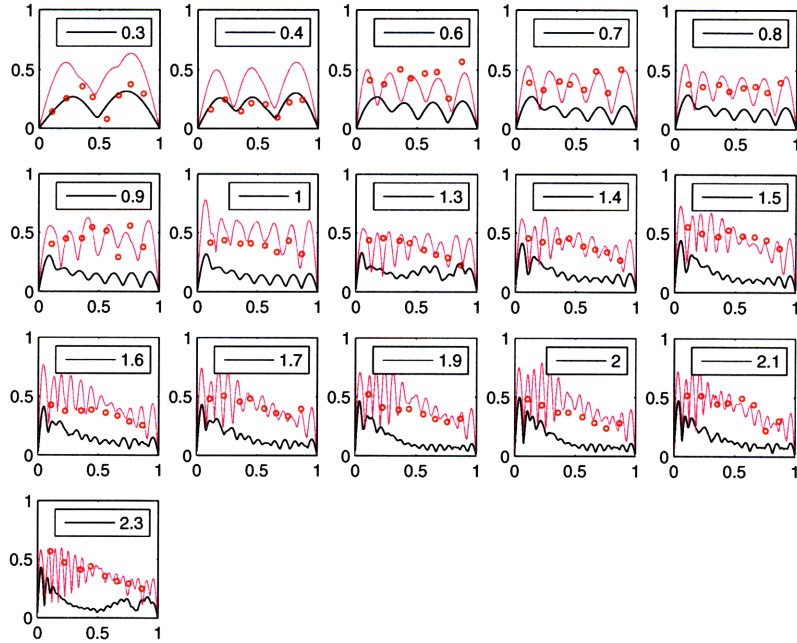
Figure B.2: Nominal (black) versus optimal (magenta) VIVA reconstructions. Abscissa is non-dimensional span, ordinate is non-dimensional displacement rms; label is flow velocity in m/s.
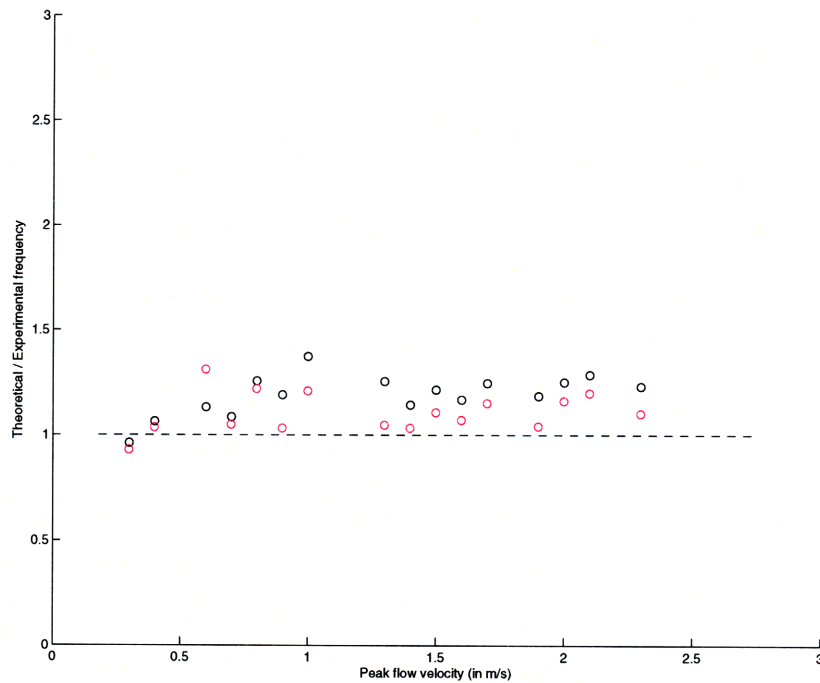
Figure B.3: Nominal (black) versus optimal (magenta) VIVA frequency comparisons.

Appendix C

Construction of the Database Transformation Function

This appendix contains the details of the construction of the database transformation function, i.e. the function $\phi(\cdot)$ that scales and translates the nominal databases.

Consider nominal straked databases $C_{lv,s}^{nom}(Vr, Y^*)$ and $C_{m,s}^{nom}(Vr, Y^*)$. We wish to obtain modified databases

$$C_{lv,s}^{mod}(Vr, Y^*) = \alpha_1^{lv} C_{lv,s}^{nom}(\alpha_2^{lv} Vr + \beta_2^{lv}, \alpha_3^{lv} Y^* + \beta_3^{lv}) + \beta_1^{lv}, \qquad (C.1)$$

and

$$C_{m,s}^{mod}(Vr, Y^*) = \alpha_1^{m} C_{m,s}^{nom}(\alpha_2^{m} Vr + \beta_2^{m}, \alpha_3^{m} Y^* + \beta_3^{m}) + \beta_1^{m}, \qquad (C.2)$$

where α_1^{lv}, α_2^{lv}, α_3^{lv}, α_1^{m}, α_2^{m}, α_3^{m} are 'reasonable' scaling parameters (for our problem, a reasonable range is $[1/3, 3]$ for example) and β_1^{lv}, β_2^{lv}, β_3^{lv}, β_1^{m}, β_2^{m}, β_3^{m} are 'reasonable' translating parameters (e.g. in the range $[-2, 2]$). It is convenient to group the parameters in parameter vectors, for example $\boldsymbol{\alpha}^{lv} = \left(\alpha_1^{lv}, \alpha_2^{lv}, \alpha_3^{lv}\right)$.

The functions $\phi_{lv}(\cdot)$ and $\phi_m(\cdot)$ are defined implicitly through the relations

$$\begin{aligned}
C_{lv,s}^{mod}(Vr, Y^*) &= \alpha_1^{lv} C_{lv,s}^{nom}(\alpha_2^{lv} Vr + \beta_2^{lv}, \alpha_3^{lv} Y^* + \beta_3^{lv}) + \beta_1^{lv} \\
&\equiv \phi_{lv}\left(C_{lv,s}^{nom}(Vr, Y^*); \alpha_1^{lv}, \alpha_2^{lv}, \alpha_3^{lv}, \beta_1^{lv}, \beta_2^{lv}, \beta_3^{lv}\right) \\
&= \phi_{lv}\left(C_{lv,s}^{nom}(Vr, Y^*); \boldsymbol{\alpha}^{lv}, \boldsymbol{\beta}^{lv}\right), \qquad (C.3)
\end{aligned}$$

and

$$C_{m,s}^{mod}(Vr, Y^*) = \alpha_1^m C_{m,s}^{nom}(\alpha_2^m Vr + \beta_2^m, \alpha_3^m Y^* + \beta_3^m) + \beta_1^m$$
$$\equiv \phi_m\left(C_{m,s}^{nom}(Vr, Y^*); \alpha_1^m, \alpha_2^m, \alpha_3^m, \beta_1^m, \beta_2^m, \beta_3^m\right)$$
$$= \phi_m\left(C_{m,s}^{nom}(Vr, Y^*); \boldsymbol{\alpha}^m, \boldsymbol{\beta}^m\right). \tag{C.4}$$

When there is no need to explicitly show the dependence on the scaling and translating parameters, we use the abbreviated $\phi_{lv}(C_{lv,s}^{nom}(Vr, Y^*))$ and $\phi_m(C_{m,s}^{nom}(Vr, Y^*))$. Lastly, we define $\phi \equiv (\phi_{lv}, \phi_m))$ to be the function that maps the nominal databases to modified databases, i.e.

$$\phi : \left(C_{lv,s}^{nom}, C_{m,s}^{nom}\right) \longrightarrow \left(C_{lv,s}^{mod}, C_{m,s}^{mod}\right), \tag{C.5}$$

which means

$$\left(C_{lv,s}^{mod}, C_{m,s}^{mod}\right) = \phi\left(\left(C_{lv,s}^{nom}, C_{m,s}^{nom}\right)\right),$$
$$\equiv \left(\phi_{lv}\left(C_{lv,s}^{nom}\right), \phi_m\left(C_{m,s}^{nom}\right)\right). \tag{C.6}$$

Appendix D

On the Nelder-Mead Simplex Method

This is an appendix on the workings of the Nelder-Mead simplex method. As mentioned in the main text, descriptions of the method can be found in many places, a good reference being Lagarias, et al. (1998), which also briefly discusses convergence properties of the algorithm for low problem dimension. What follows in this appendix is an adaptation from the aforementioned paper.

The Nelder-Mead method is an algorithm for minimizing a function $f : \mathbb{R}^n \longrightarrow \mathbb{R}$. It depends on the so-called coefficients of reflection ($\rho > 0$), expansion ($\chi > \min(\rho, 1)$), contraction ($1 > \gamma > 0$) and shrinkage ($1 > \sigma > 0$). Standard values for these coefficients are $\rho = 1, \chi = 2, \gamma = 1/2, \sigma = 1/2$.

The algorithm begins with a non-degenerate simplex in $\mathbb{R}^n$ defined by points $\mathbf{x}_1, ..., \mathbf{x}_{n+1}$. It then moves through n-dimensional space via a series of simplices until a local optimum has been found. Let us describe one typical iteration of the algorithm.

1. **Order simplex points.** Order the $n+1$ vertices of the current simplex such that $f(\mathbf{x}_1) \leq ... \leq f(\mathbf{x}_{n+1})$.

2. **Find the simplex centroid.** Calculate $\overline{\mathbf{x}} = \frac{1}{n} \sum_{i=1}^{n} \mathbf{x}_i$, the centroid of the n best points.

3. **Reflect.** Find the reflection point $\mathbf{x}_r = \overline{\mathbf{x}} + \rho\left(\overline{\mathbf{x}} - \mathbf{x}_{n+1}\right)$ and its value $f\left(\mathbf{x}_r\right)$. If $f(\mathbf{x}_n) > f\left(\mathbf{x}_r\right) \geq f(\mathbf{x}_1)$, form a new simplex by replacing $\mathbf{x}_{n+1}$ by $\mathbf{x}_r$ in the current simplex and go to the next iteration; otherwise, go to Step 4.

4. **Expand.** If $f(\mathbf{x}_1) > f\left(\mathbf{x}_r\right)$ in Step 3, calculate the expansion point $\mathbf{x}_e = \overline{\mathbf{x}} + \chi\left(\mathbf{x}_r - \overline{\mathbf{x}}\right)$ and its value $f\left(\mathbf{x}_e\right)$. If $f(\mathbf{x}_r) > f\left(\mathbf{x}_e\right)$, form a new simplex by replacing $\mathbf{x}_{n+1}$ by $\mathbf{x}_e$ in the current simplex and go to the next iteration; otherwise, go to Step 5.

5. **Contract.**

   Contract outside. If $f(\mathbf{x}_{n+1}) > f\left(\mathbf{x}_r\right) \geq f\left(\mathbf{x}_n\right)$ in Step 3, calculate the outside contraction point $\mathbf{x}_{oc} = \overline{\mathbf{x}} + \gamma\left(\mathbf{x}_r - \overline{\mathbf{x}}\right)$ and its value $f\left(\mathbf{x}_{oc}\right)$. If $f(\mathbf{x}_r) \geq f\left(\mathbf{x}_{oc}\right)$, form a new simplex by replacing $\mathbf{x}_{n+1}$ by $\mathbf{x}_{oc}$ in the current simplex and go to the next iteration; otherwise, go to Step 6.

   Contract inside. If $f(\mathbf{x}_r) \geq f\left(\mathbf{x}_{n+1}\right)$ in Step 3, calculate the inside contraction point $\mathbf{x}_{ic} = \overline{\mathbf{x}} - \gamma\left(\overline{\mathbf{x}} - \mathbf{x}_{n+1}\right)$ and its value $f\left(\mathbf{x}_{ic}\right)$. If $f(\mathbf{x}_{n+1}) > f\left(\mathbf{x}_{ic}\right)$, form a new simplex by replacing $\mathbf{x}_{n+1}$ by $\mathbf{x}_{ic}$ in the current simplex and go to the next iteration; otherwise, go to Step 6.

6. **Shrink.** Calculate the n points $\mathbf{v}_i = \mathbf{x}_1 + \sigma\left(\mathbf{x}_i - \mathbf{x}_1\right), i = 2, \ldots n+1$ and their values $f(\mathbf{v}_2), \ldots, f(\mathbf{v}_{n+1})$. Let the new simplex be the one defined by vertices $\mathbf{x}_1, \mathbf{v}_2, \ldots, \mathbf{v}_{n+1}$ and go to the next iteration.

Tie breaking rules when equal function values arise do exist but there is no point in listing them here. What is more instructive is to visualize the Nelder-Mead steps when $n = 2$ (Figure D.1).

We close by noting that, for our purposes, the algorithm here presented is used to solve (I.16), which reads

$$\min_{\phi} \frac{1}{|\mathcal{D}||\mathcal{A}|} \sum_{d \in \mathcal{D}} \sum_{a \in \mathcal{A}} \left| (Y^*_{rms})_d \left(z^*_a; C^{opt}_{lv,b}, C^{opt}_{m,b}, \phi\left(C^{nom}_{lv,s}, C^{nom}_{m,s} \right) \right) - (Y^*_{rms})^{exp}_{a,d} \right|. \tag{D.1}$$

In view of Appendix B, (D.1) is equivalent to

$$\min_{\boldsymbol{p}} J\left(\boldsymbol{p}\right), \tag{D.2}$$

where

$$\boldsymbol{p} = (\boldsymbol{\alpha}^{lv}, \boldsymbol{\beta}^{lv}, \boldsymbol{\alpha}^m, \boldsymbol{\beta}^m), \tag{D.3}$$

and

$$J\left(\boldsymbol{p}\right) =$$

$$\frac{1}{|\mathcal{D}|\,|\mathcal{A}|} \sum_{d\in\mathcal{D}} \sum_{a\in\mathcal{A}} \left| (Y_{rms}^*)_d \left(z_a^*; C_{lv,b}^{opt}, C_{m,b}^{opt}, \phi\left(C_{lv,s}^{nom}, C_{m,s}^{nom}; \boldsymbol{p}\right)\right) - (Y_{rms}^*)_{a,d}^{exp} \right|.$$

$$(D.4)$$

Note that Equation (D.2) is a minimization of a function (J) over a 12-dimensional parameter space; hence, the Nelder-Mead algorithm may be used.
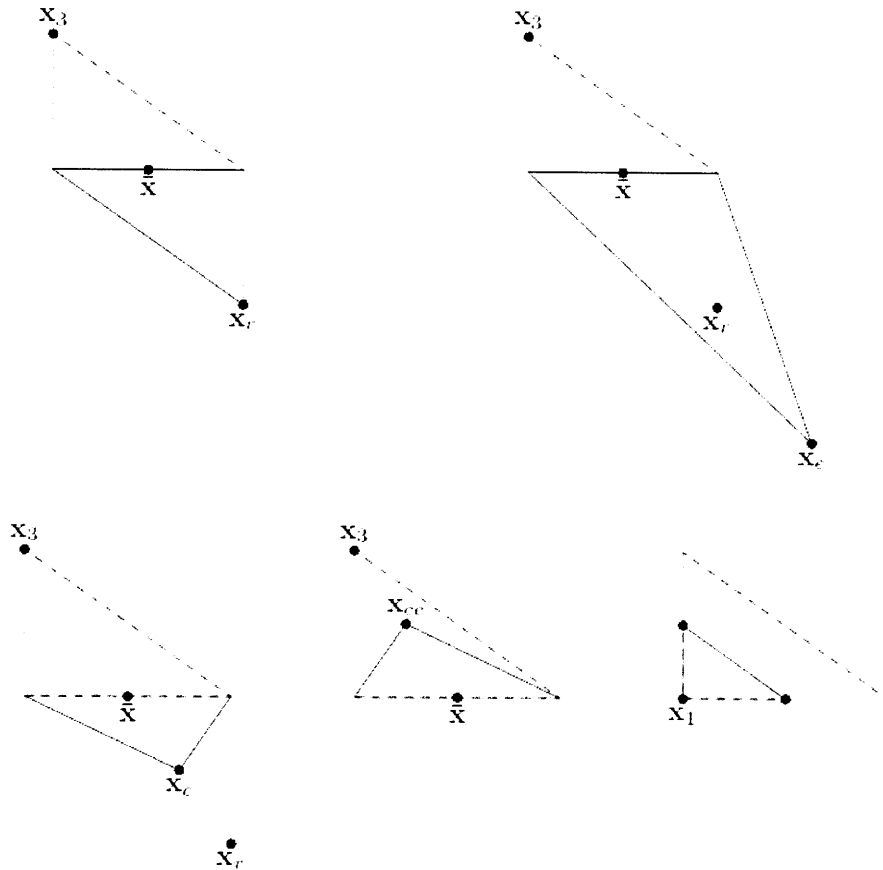
Figure D.1: Steps of the Nelder-Mead simplex method. The original simplices are shown with a dashed lines. The modified simplices after a reflection, expansion, outside contraction, inside contraction and shrinkage are shown with solid lines. (Figure adapted from Lagarias, et al. (1998).)

Appendix E

VIVOS: A Program for Extracting Optimal Force Databases from VIV Experiments

The VIV optimization suite (VIVOS) modifies the nominal lift coefficient databases in such way as to have best agreement between theoretically predicted and experimentally measured riser response. The program uses experimental data from real marine risers to calibrate the force databases obtained from laboratory experiments on small rigid cylinders (the original databases are referred to as the nominal databases, while the modified databases resulting from the optimization are referred to as the optimal databases). VIVOS is written in MATLAB, but often calls VIVA which is written in FORTRAN. The structure of this manual is as follows: Section 2 briefly describes the functions of the main subroutines; Section 3 is on program inputs; Section 4 explains how to run the program; finally, Section 5 is on program outputs.

run_VIVOS.m
run_MISC_clearold.m
get_OPT_inputdata.m
"DATASET".m | TEMP_"DATASET"_inputs.mat
get_OPT_parameters.m | TEMP_param_range_bare.mat
TEMP_param_range_strake.mat
TEMP_Jall_wt.mat
TEMP_bare_opt_bool.mat
TEMP_strake_opt_bool.mat
TEMP_nmsimplex_inputs.mat
TEMP_dataset.mat
get_OPT_main_databases.m
write_VIVA_inputs.m
get_VIVA_inputs.m | get_DATA_flow_velocity.m
VIVAinputdata_XXXX.mat
write_VIVARISPRE.m | RISPRE.IN
write_VIVARISDYN.m | RISDYN-N.IN
write_VIVACONDITIONS.m | CONDITIONS.IN
write_VIVARISFAT.m | RISFAT.IN
write_VIVANO_FILES.m | no_files.IN
get_VIVA_modes_nominal.m
get_PARAM_nominalclvcm.m | TEMP_bare_data_clv_cm.mat
TEMP_straked_data_clv_cm.mat
write_CMandCLV_FREEVIVA.m | write_VIVA_bare_database_param.m | get_PARAM_clv_cm_freeviva.m | get_PARAM_curveintersect.m
get_PARAM_hmmovavg.m
basic_bare
TEMP_bare_clvastar.mat
TEMP_bare_file_matrix_param.mat
write_VIVA_straked_database_lin.m | file_js.dat
TEMP_straked_file_matrix_lin.mat
run_VIVA_once.m | BISPREP.exe
RISG.exe
VIVA211ULDR.exe
NDP_normcomplexmodes.mat
plot_VIVA_modes_nominal.m | get_DATA_flow_velocity.m
get_DATA_exp_mode_frequency.m
disp_rms_nom.fig
freq1_nom.fig
freq2_nom.fig
digidata_VIVA_disp_nom_XXXX.OUT
digidata_freq_nom_XXXX.OUT
digidata_EXP_disp_XXXX.OUT
run_OPT_NMSIMPLEX.m | run_evaluateJ.m | ....(see next page)................
SOLN_param_time.mat
SOLN_param.mat
TEMP_bool.mat
TEMP_Jall_NM.mat
plot_VIVA_modes_modified.m | get_DATA_flow_velocity.m
get_DATA_exp_mode_frequency.m
run_evaluateJ.m | ....(see next page)................
disp_rms_nom_opt.fig
freq1_nom_opt.fig
freq2_nom_opt.fig
digidata_VIVA_disp_opt_XXXX.OUT
digidata_freq_opt_XXXX.OUT
error_metric.OUT
basic_bare_opt
file_js_opt
TEMP_param_best.mat
plot_OPT_databases.m | get_PARAM_modifyclvcm.m | get_PARAM_param.m | get_PARAM_clvnineparam.m | get_PARAM_extrapolateclv.m
get_PARAM_clvsecondpeak.m
get_PARAM_cleanmod.m
get_PARAM_extrapolatecm.m
get_PARAM_cmthreeparam.m
get_PARAM_lin.m
TEMP_bare_data_clv_cm.mat
TEMP_straked_data_clv.mat
TEMP_straked_data_cm.mat
clv_bare_nom.fig
cm_bare_nom.fig
clv_straked_nom.fig
cm_straked_nom.fig
clv_bare_opt.fig
cm_bare_opt.fig
clv_straked_opt.fig
cm_straked_opt.fig
TEMP_param_new.mat
VIVOS_inputs.mat

Key
Matlab fctn
VIVA fctn
VIVA input file
Program output
TEMP file output

Figure E.1: Code tree: main program.

run_evaluateJ.m
get_DATA_exp_mode_frequency.m
get_PARAM_modifyclvcm.m | get_PARAM_param.m | get_PARAM_clvnineparam.m | get_PARAM_extrapolateclv.m
get_PARAM_clvsecondpeak.m
get_PARAM_cleanmod.m
get_PARAM_extrapolatecm.m
get_PARAM_cmthreeparam.m
get_PARAM_lin.m
TEMP_bare_data_clv_cm.mat
TEMP_straked_data_clv.mat
TEMP_straked_data_cm.mat
write_CMandCLV_FREEVIVA.m | write_VIVA_bare_database_param.m | get_PARAM_clv_cm_freeviva.m | get_PARAM_curveintersect.m
get_PARAM_hmmovavg.m
basic_bare
TEMP_bare_clvastar.mat
TEMP_bare_file_matrix_param.mat
write_VIVA_straked_database_lin.m | file_js.dat
TEMP_straked_file_matrix_lin.mat
run_VIVA_once.m | BISPREP.exe
RISG.exe
VIVA211ULDR.exe
NDP_normcomplexmodes.mat
SOLN_Jall_HM.mat
TEMP_param_new.mat
TEMP_zmodes.mat
TEMP_bool.mat

Key
Matlab fctn
VIVA fctn
VIVA input file
Program output
TEMP file output

Figure E.2: Code tree: main function.

74

get_DATA_exp_mode_frequency.m	....	function to extract the experimental displacement rms and peak frequency
get_DATA_flow_velocity.m	....	function to extract the experimental velocity profile
get_MISC_insertrow.m	....	function to insert vector b at row location n
get_OPT_inputdata.m	....	function to read basic dataset info and define optimization parameters
get_OPT_main_databases.m	....	function to obtain nominal and optimal VIVA solutions
get_OPT_parameters.m	....	function to read optimization parameters
get_PARAM_cleanmod.m	....	function to clean the modified data and bring it into a format compatible with VIVA
get_PARAM_clv_cm_freeviva.m	....	function to obtain the Clv and Cm in the format required by VIVA
get_PARAM_clvnineparam.m	....	function to output the new Clv matrix from the input values of the parameters
get_PARAM_clvsecondpeak.m	....	function to add the second peak in the Clv
get_PARAM_cmthreeparam.m	....	function to output the new Cm matrix from the input values of the parameters
get_PARAM_curveintersect.m	....	function to find the point of intersection of two curves
get_PARAM_extrapolateclv.m	....	function to obtain a similified global shape of the Clv surface
get_PARAM_extrapolatecm.m	....	function to obtain a similified global shape of the Cm surface
get_PARAM_hmmovavg.m	....	function to obtain the moving average of a signal
get_PARAM_lin.m	....	function to scale and shift Cl surfaces
get_PARAM_modifyclvcm.m	....	function to modify the Clv and Cm databases
get_PARAM_nominalclvcm.m	....	function to get the nominal databases
get_PARAM_param.m	....	function to get the Clv and Cm parameters
get_VIVA_inputs.m	....	function to define the experimental setting
get_VIVA_modes_nominal.m	....	function to obtain the nominal VIVA modes
plot_OPT_databases.m	....	function to plot the nominal and optimal database surfaces and VIVA files
plot_VIVA_basicbare.m	....	function to plot the basic_bare file
plot_VIVA_filejs.m	....	function to plot the file_jd.dat file
plot_VIVA_modes_modified.m	....	function to plot the optimal VIVA solution and store several output files and figures
plot_VIVA_modes_nominal.m	....	function to plot the nominal VIVA solution
run_evaluateJ.m	....	function to evaluate the optimization index for each input parameter vector
run_MISC_clearold.m	....	function to remove old directories
run_OPT_NMSIMPLEX.m	....	function to perform the optimization using the NM method
run_VIVA_once.m	....	function to run VIVA codes and store outputs
run_VIVOS.m	....	program to obtain the optimal Clv and Cm coefficients from experiments
Sheared_17_5_41.m	....	
Sheared_bare.m	....	
Uniform_17_5_41.m	....	
Uniform_bare.m	....	
write_CMandCLV_FREEVIVA.m	....	function to write the nominal and optimal force databases
write_VIVA_bare_database_param.m	....	function to write the basic_bare file
write_VIVA_inputs.m	....	function to write the VIVA input files
write_VIVA_straked_database_lin.m	....	function to write the file_js.dat file
write_VIVACONDITIONS.m	....	function to write the CONDITIONS input file for VIVA
write_VIVANO_FILES.m	....	function to write the no_files input file for VIVA
write_VIVARISDYN.m	....	function to write the RISDYN input file for VIVA
write_VIVARISFAT.m	....	function to write the RISDYN input file for VIVA
write_VIVARISPRE.m	....	function to write the RISPRE input file for VIVA
VIVOS_inputs.mat	....	

Figure E.3: List of programs.

E.1 Program hierarchy

The easiest and most efficient way to describe the use of the program is through example and reference to the code trees of Figures E.1 - E.2 and the file descriptions of Figure E.3. In particular, assume you wanted to update the existing bare lift coefficient databases using data from the NDP Sheared_bare dataset. The dataset comprises of 22 datacases spanning a range of maximum flow velocities from 0.3 to $2.4m/s$ in increments of $0.1m/s$ (roughly).

The program starts by reading the input data (function get_OPT_inputdata.m): basic dataset inputs are read (function Sheared_bare.m) and the optimization parameters are loaded (function get_OPT_parameters.m). The program then proceeds to find the optimal databases (function get_OPT_main_databases.m). First, the VIVA input files for each datacase in the dataset are written and stored in the INPUTS folder (function write_VIVA_inputs.m). Second, the VIVA nominal modes are found (function get_VIVA_modes_nominal.m) and plotted (function plot_VIVA_modes_nominal.m). Next, the optimization is carried out (function run_OPT_NMSIMPLEX.m). The optimization algorithm recursively evaluates the deviations between theoretical and experimental response (function run_evaluateJ.m). When the optimization is finished, the optimal VIVA modes and optimal force databases are plotted and stored (functions plot_VIVA_modes_modified.m and plot_OPT_databases.m respectively). All outputs are stored in the OUTPUTS folder.

E.2 Program inputs

1. Experimenal data: Create a folder named Sheared_bare (the dataset name) in the DATA folder. Create subfolders 2310, 2320, ..., 2510 (the tags of the datacases) within the Sheared_bare folder.[1] For each datacase XXXX (XXXX = 2310, 2320, ..., 2510), give a mat-file CF_rms_XXXX.mat with the following:

    (a) z_exp_meas - locations of the measurement points (non-dimensionalized by the riser's span)

---

[1]Limit the number of datacases per dataset to 25.

(b) Yn_exp_meas - cross-flow displacement rms measured at the measurement points z_exp_meas (non-dimensionalized by the riser's diameter)

(c) fn_exp - peak 1st harmonic frequency (in Hz)

(d) z_exp_vel - locations along the riser where the flow velocity is measured (non-dimensionalized by the riser's span)

(e) VCF_exp - cross-flow current speed at points z_exp_vel (in m/s)

(f) VIL_exp - in-line current speed at points z_exp_vel (in m/s)

2. Basic dataset information: Create an m-file named after the dataset (here Sheared_bare.m) and provide the datacase tags, as well as the riser length and diameter; extensive commenting throughout the m-file helps you do this.

3. VIVA input files: Open get_VIVA_inputs.m and provide all the riser structural properties needed to run VIVA; extensive commenting throughout the m-file helps you do this.

4. Basic optimization parameters: Open get_OPT_parameters.m and change the optimization parameters as desired. (Note: this is optional; the algorithm works fine with the parameters already provided therein.)

E.3   Running the program

Run the program by typing (in the command window of MATLAB):

>> run_VIVOS(dataset,bare_opt_bool,strake_opt_bool), where

1. dataset - the name of the dataset employed

2. bare_opt_bool - a boolean that equals 1 if the bare databases are to be optimized, and 0 otherwise

3. strake_opt_bool - a boolean that equals 1 if the straked databases are to be optimized, and 0 otherwise

Hence, if you want to use the Sheared_bare dataset to obtain optimal bare databases, type:

>> run_VIVOS('Sheared_bare',1,0).

The program contains the data and input files for 4 datasets from the NDP experiments: Sheared_bare, Uniform_bare, Sheared_17_5_41, and Uniform_17_5_41.

E.4   Program outputs

1. Measured and predicted response data: For each datacase XXXX, there is a subfolder named XXXX in the OUTPUTS folder which contains:

   (a) digidata_EXP_disp_XXXX.OUT - has non-dimensional span in first column, measured non-dimensional cross-flow displacement rms in second

   (b) digidata_VIVA_disp_nom_XXXX.OUT - has non-dimensional span in first column, nominal VIVA-predicted non-dimensional cross-flow displacement rms in second

   (c) digidata_freq_nom_XXXX.OUT - contains the observed peak 1st harmonic frequency and the nominal VIVA-predicted peak frequency (in Hz)

   (d) digidata_VIVA_disp_opt_XXXX.OUT - has non-dimensional span in first column, optimal VIVA-predicted non-dimensional cross-flow displacement rms in second

   (e) digidata_freq_opt_XXXX.OUT - contains the observed peak 1st harmonic frequency and the optimal VIVA-predicted peak frequency (in Hz)

2. Error metric: The file error_metric.OUT in the OUTPUTS folder contains the values of error metric before and after optimization.

3. Database files: Nominal VIVA force database files (basic_bare_nom and file_js_nom) and optimal VIVA force database files (basic_bare_opt and file_js_opt) can be found in the VIVA folder.

4. Figures: The OUTPUS folder contains several figures (both in fig and pdf format):

(a) Figures that compare VIVA performance against experimental data before and after optimization:

    i. disp_rms_nom.fig/pdf and disp_rms_nom_opt.fig/pdf

    ii. freq1_nom.fig/pdf and freq1_nom_opt.fig/pdf

    iii. freq2_nom.fig/pdf and freq2_nom_opt.fig/pdf

(b) Figures of the nominal and optimal force database surfaces:

    i. clv_bare_nom.fig/pdf, cm_bare_nom.fig/pdf, clv_bare_opt.fig/pdf, and cm_bare_opt.fig/pdf

    ii. clv_straked_nom.fig/pdf, cm_straked_nom.fig/pdf, clv_straked_opt.fig/pdf, and cm_straked_opt.fig/pdf (if relevant)